2015

SINGLE PHASE MULTILEVEL INVERTER FOR GRID-TIED PHOTOVOLTAIC SYSTEMS

Martin Edward Prichard
University of Kentucky, prichard.martin@gmail.com

STUDENT AGREEMENT:

I represent that my thesis or dissertation and abstract are my original work. Proper attribution has been given to all outside sources. I understand that I am solely responsible for obtaining any needed copyright permissions. I have obtained needed written permission statement(s) from the owner(s) of each third-party copyrighted matter to be included in my work, allowing electronic distribution (if such use is not permitted by the fair use doctrine) which will be submitted to UKnowledge as Additional File.

I hereby grant to The University of Kentucky and its agents the irrevocable, non-exclusive, and royalty-free license to archive and make accessible my work in whole or in part in all forms of media, now or hereafter known. I agree that the document mentioned above may be made available immediately for worldwide access unless an embargo applies.

I retain all other ownership rights to the copyright of my work. I also retain the right to use in future works (such as articles or books) all or part of my work. I understand that I am free to register the copyright to my work.

REVIEW, APPROVAL AND ACCEPTANCE

The document mentioned above has been reviewed and accepted by the student's advisor, on behalf of the advisory committee, and by the Director of Graduate Studies (DGS), on behalf of the program; we verify that this is the final, approved version of the student's thesis including all changes required by the advisory committee. The undersigned agree to abide by the statements above.

Martin Edward Prichard, Student

Dr. Aaron Cramer, Major Professor

Dr. Caicheng Lu, Director of Graduate Studies

SINGLE PHASE MULTILEVEL INVERTER FOR GRID-TIED PHOTOVOLTAIC SYSTEMS

THESIS

A thesis submitted in partial fulfillment of the
requirements for the degree of Master of Science in Electrical Engineering
in the College of Egineering
at the University of Kentucky

By

Martin Edward Prichard

Lexington, Kentucky

Director: Dr. Aaron Cramer, Assistant Professor of Electrical and Computer Engineering

Lexington, Kentucky

2015

ABSTRACT OF THESIS

SINGLE PHASE MULTILEVEL INVERTER
FOR PHOTOVOLTAIC SYSTEMS

Multilevel inverters offer many well-known advantages for use in high-voltage and high-power applications, but they are also well suited for low-power applications. A single phase inverter is developed in this paper to deliver power from a residential-scale system of Photovoltaic panels to the utility grid. The single-stage inverter implements a novel control technique for the reversing voltage topology to produce a stepped output waveform. This approach increases the granularity of control over the PV systems, modularizing key components of the inverter and allowing the inverter to extract the maximum power from the systems. The adaptive controller minimizes harmonic distortion in its output and controls the level of reactive power injected to the grid. A computer model of the controller is designed and tested in the MATLAB program Simulink to assess the performance of the controller. To validate the results, the performance of the proposed inverter is compared to that of a comparable voltage-sourced inverter.

KEYWORDS: Multilevel Inverter, Microinverter, Grid-tied Photovoltaic Systems, Low Power Solar Energy, Reversing Voltage Topology

_____Martin Prichard_____

_____October, 23 2015_____

SINGLE PHASE MULTILEVEL INVERTER
FOR PHOTOVOLTAIC SYSTEM

By

Martin Edward Prichard

Dr. Aaron Cramer
Director of Thesis

Dr. Caicheng Lu
Director of Graduate Studies

October 23, 2015

This work is dedicated to Kara Beer and my parents, Bennett and Louis Prichard.

ACKNOWLEDGEMENTS

I would like express my deep gratitude to Dr. Aaron Cramer, my advisor, for his valuable and constructive suggestions during the planning and development of this work as well as his patient guidance throughout the process. I would like to thank Dr. Larry Holloway and Dr. Vijay Singh for their time and input as members of my thesis committee. I offer a special thanks to the University of Kentucky and its Department of Electrical Engineering for giving me the opportunity to write this thesis. I am particularly grateful for the encouragement from my friends and the support from my family and loved ones. Without them, none of this would have been possible.

TABLE OF CONTENTS

LIST OF TABLES

LIST OF FIGURES

1 Introduction

Due to the industrialization of developing countries, the increasing worldwide population, and the overall desire for an improved quality of life, there is an ever-increasing global demand for electrical power. Combustible fossil fuels and nuclear sources account for approximately three quarters of the electricity produced globally; however, these supplies are limited [1,2,3]. Due to the finite nature of these resources, researchers are interested in generating power from renewable sources in order to find a more environmentally sustainable way to produce electricity. Through advances in technology and manufacturing techniques, photovoltaic (PV) cells that harvest solar energy have become economically competitive with other technologies that generate power from renewable sources.

While PV systems can be installed in a centralized generating facility, they are uniquely suited for distributed generation applications. Solar farms use PV cells to generate large quantities of power in a single location. They are comparable to the generating facilities of more traditional fuels, but less efficient from an energy density (power produced per square foot of land occupied) point of view. Due to safety and aesthetic concerns associated with traditional generation facilities, they are often constructed away from heavily populated areas. The electricity produced at these facilities must be transmitted long distances to the end user, which requires a costly, complex infrastructure and exposes the entire system to higher levels of power loss and security risks. Conversely, PV systems can produce power closer to the end user, albeit in smaller quantities. PV cells do not benefit from the same economy of scale as traditional generation technologies and thus generally do not become more effective when cells are conglomerated or enlarged. Their small packaging and the widespread presence of the fuel source, sunlight, makes solar power especially attractive for geographically distributed residential and commercial applications.

All practical PV panels require power converters to transform the electricity they produce into a more useful form. There are many different types of converters due to the wide variety of loads that PV systems serve, including inverters, which are used to connect PV systems to the utility grid. Some of these inverters have been designed specifically for systems that produce small quantities of power, such as residential rooftop units. A key focus for low-power solar systems is to provide as much power to the end user as possible. Two basic strategies exist to accomplish this task: maximize power generated by the PV panel and reduce power consumed by the inverter. The inverter introduced in this paper combines both strategies to maximize power delivered to the utility grid. Ease of installation is another factor that is increasingly important to customers. Micro inverters specifically are pushing towards modular plug-and-play units that make installation less complicated by combining the PV panel and inverter into one package instead of providing the two as separate products

A single phase inverter is developed in this paper that connects PV systems to the utility grid. This inverter produces a grid-level output voltage at power levels lower than 2 kW. Unlike many traditional grid-tied PV inverters, the proposed inverter does not generate a higher DC voltage than the use a PWM or VSI based inverter to produce an AC voltage. Rather, the inverter continually changes the number of PV systems connected in a series with one another to produce a stepped output waveform that closely resembles a sinusoid. The inverter is similar to other micro inverters in that it is designed to be modular in nature and can be manufactured into the PV panel itself, allowing for direct plug-and-lay capabilities. Relative to other comparable micro inverters, the proposed inverter offers several advantages: having fewer components, consuming less power, and generating less harmonic distortion in its outputs.

Part I of this paper introduces a single-phase, grid-tied inverter for PV systems. Part II explains why an inverter is required to connect the PV system to the utility grid. It also addresses

several benefits associated with VSI inverters in particular before describing micro inverters and reasons why they have become more popular in recent years. Lastly, there is a brief summary of the Fourier series and harmonics. Part III describes the proposed inverter and explains how a computer model of the inverter is developed in the Matlab program Simulink. Next, Part IV assesses the performance of the inverter. It documents the output of the inverter in absolute terms before weighing its performance with that of a comparable inverter using a VSI-based controller. Lastly, Part V concludes with a summary of arguments and discusses potential opportunities for this proposed technology moving forward.

2 Conceptual Development

A fundamental description of photovoltaic devices is given. General techniques and circuit topologies used to connect photovoltaic devices to the utility grid are discussed. Methods to analyze harmonic content are provided.

2.1 Photovoltaic Devices

Energy exists in many forms, and it is often helpful or even necessary to convert it from one form to another. The radiant energy that comes from the sun is naturally converted into thermal energy by certain objects as they absorb the sunlight. In 1839, Edmond Becquerel observed that some materials convert sunlight into electricity, the process of which is commonly referred to as the photovoltaic effect [4]. Since then, humans have attempted to harness and exploit this phenomenon. In the 1950's, a team of scientists at Bell Laboratories introduced one of the first devices that produced a useful amount of electricity when exposed to sunlight: a silicon solar cell [5].

A solar cell, also called a photovoltaic (PV) cell, produce electricity when it absorbs sunlight. The absorbed light excites an electron and breaks the covalent bonds holding it in place. The electromagnetic field inherent to the structure of the cell sweeps the freed electron away from its location. With exposure to significant amounts of sunlight, enough electrons are swept away so that a steady flow of electrons establishes an electric current.

The P-N junction is the fundamental structure within the PV cell that produces the electromagnetic field mentioned above. In many practical devices, N-type and P-type semiconductor materials are often layered on top of one another, and the point of contact between the two materials is called the P-N junction. The different electrical properties of the semiconductors produce an electromagnetic field across the junction, which allows the PV cell to

convert sunlight into a useful amount of electricity as described in the previous paragraph. This field creates a non-linear relationship between the current flowing through the junction and the voltage potential across it.

2.1.1 Output Characteristics

The current produced by a PV cell has a unique correlation to the voltage across its output terminals because the P-N junction is the heart of the PV cell. This distinct relationship is depicted in Figure 2.1a.

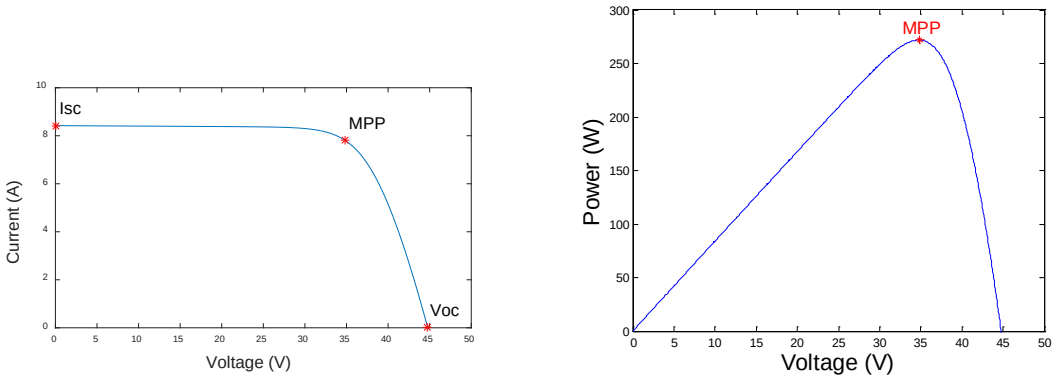

(a) (b)

Figure 2.1: Typical (a) I-V and (b) P-V curves associated with the output of a PV panel

The relationships between a PV panel's output current, voltage, and power are complex and non-linear. It is difficult and sometimes unnecessary to attempt to know the exact coordinates of every point on the curve; however, there are three important points that are commonly used to describe the curve. Two straightforward points are the short circuit current (I_{sc}, current when Voltage = 0 V) and the open circuit voltage, (V_{oc}, voltage when Current = 0 A). These aspects are important to the design of the system as they represent the maximum levels of current and voltage that the PV panel can produce. There is a single point on the I-V curve that produces the maximum amount of power possible. This point is known as the maximum power

point, MPP. Controllers attempt to make the PV system operate near the MPP to maximize the yields and efficiency of the system.

Values for these important voltages and currents can be determined experimentally but are often provided on the manufacturer's data sheet. The data sheet values portray the panel's performance when exposed to standard test conditions, STC. STC defines cell temperature (T_{ref} = 25 °C), solar spectrum (AM_{ref} = 1.5) and solar irradiance (G_{ref} = 1000 W/m_2) in accordance with IEC 60904 standards [6]. Solar spectrum corresponds to the length of the path that light took through the atmosphere. Solar irradiance quantifies the power per unit area produced by the sun. The panel will perform differently when any of these conditions change and the I-V and P-V curves will shift. Figure 2.2 shows the varying performance of a PV panel under different lighting conditions.

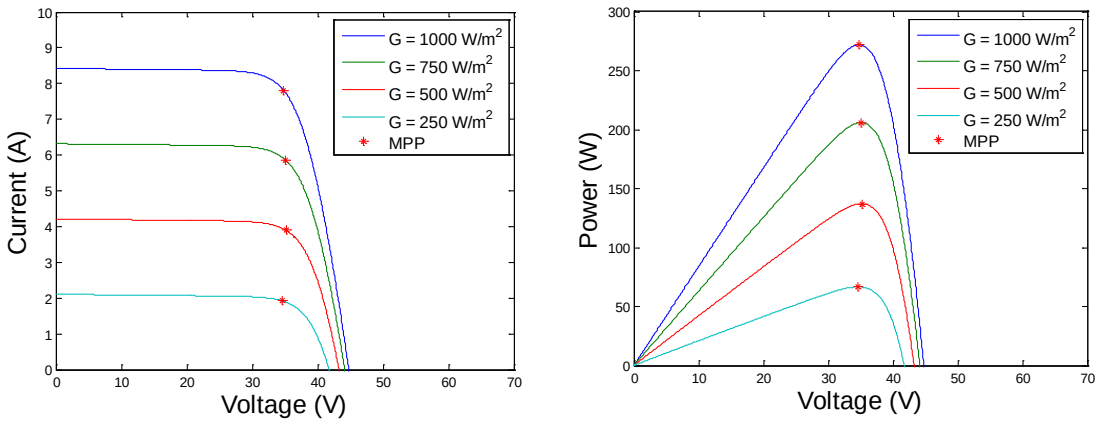

(a) (b)

Figure 2.2: The effect of different levels of solar irradiance on (a) the I-V and (b) the P-V curves

The ability to predict the outputs produced by a PV panel subject to certain conditions is extremely important to the design and operation of PV systems. An individual panel will produce different levels of power in different geographic locations because the solar panel receives

different levels of light in different parts of the world. It is necessary to know how much power a single panel will produce in order to include enough PV panels in the system to meet the needs of the load. Large PV farm operators use that knowledge to accurately estimate the amount of power they can produce to improve grid-level energy planning. Significant amounts of research have been dedicated to developing computer models that can accurately predict the output of a PV panel based on levels of solar irradiance and temperature. Some of these techniques will be discussed in in the Methodology section.

2.1.2 Maximum Power Point Tracking

From Figure 2.2 it is clear that the MPP shifts as performance of the PV panel changes, and the ability to identify the location of the MPP at any given time is paramount. Knowledge of the MPP allows the inverter to draw the appropriate voltage and current from the panel to extract all the power that it produces. Operating at the MPP maximizes the efficiency of the panel. Determining where the MPP lies is not straightforward because of the complex relationship between the PV module's output current and voltage. Often times a specific technique is chosen to determine where the MPP lies.

Certain techniques have been developed to continuously identify the location of the MPP, even when it moves. Following the MPP like in this fashion is a process known as maximum power point tracking, MPPT. It is difficult to perform MPPT analytically for real world applications of PV systems. As a result, there exist several different methods commonly used to perform MPPT. Some of the more common MPPT techniques include perturb and observe [7], ripple correlation control [8], incremental conductance method, fuzzy logic method [9] and neural network [10]. These strategies, and the majority of others, are dynamic in nature; they observe the output of the PV module and respond in a way that causes the module's operating point to shift towards the MPP.

While the details behind different MPPT strategies are interesting, there is no need to elaborate on the previously mentioned methods as that task lies outside the scope of this paper. For demonstration purposes, the means in which MPPT is performed per se is not as much of a concern as the fact that MPPT occurs. Furthermore, the MPPT technique employed in the proposed inverter is described in the Methodology section. A more effective strategy could potentially be employed to increase the performance of the inverter; however, the MPPT technique used in this paper is sufficient. As with the majority of MPPT strategies, the technique used in this paper analyzes the output of the PV module then adjusts the inverter's operation to change the amount of voltage or current drawn by the inverter. Changing the way the inverter draws voltage or current from the PV modules changes the amount of power drawn by the inverter and thus the amount of power delivered by the PV system. Thus, MPPT is adequately satisfied because the PV panel is consistently changing its operating point so that it delivers nearly all the power it is capable of producing under the given conditions.

2.2 Grid-tied Inverters for PV Systems

An inverter is a circuit or device that serves as the interface to deliver power from a DC source to an AC load. It is often desirable to produce AC power because of its compatibility with common appliances and its ability to connect to a utility grid. Inverters are often identified by the nature of their input power source: voltage-sourced inverters have sources that resemble a DC voltage source and current-sourced inverters have sources that resemble a DC current source. Industrial settings favor voltage-sourced inverters as they generally have superior efficiency, reliability and dynamic response times [11].

2.2.1 Energy Conversion: DC to AC

A voltage-sourced inverter converts power from a DC voltage source and its output effectively serves as an AC current source. The fundamental circuitry involved in this conversion is known as a full-bridge inverter, also called an H-bridge inverter, and is shown in the figure below. In accordance with Kirchhoff's Voltage Law, (KVL) the voltage source cannot be shorted; thus switches 1,1 and 2,1 cannot both be closed at the same time, and the same is true for switches 1,2 and 2,2. If switch 1,1 and 2,2 are both closed then the output, V_{out}, will be the positive DC voltage. If switch 2,1 and 1,2 are both closed then then the output will be the negative value of the DC voltage. In any other scenario, the output will be zero.

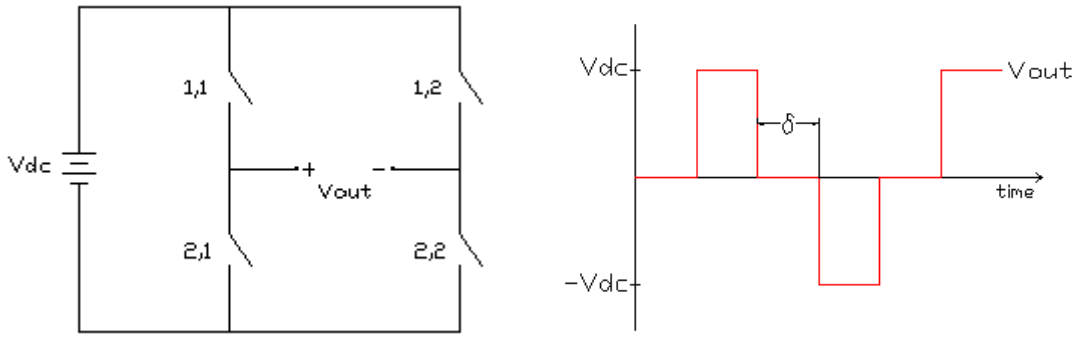

(a) Electrical Circuit (b) Output voltage

Figure 2.3: Full-bridge voltage-sourced inverter

The H-bridge topology is capable of producing an alternating value across its output terminals, which can be vaguely similar to the desired sinusoidal waveform. Different control strategies are applied to the switches to produce the desired output. The most basic inverters produce an output voltage at one of two values: the positive or negative value of the DC input. Three level inverters are quite common as well; their output can be zero volts in addition to the positive and negative value of the DC input, as shown in Figure 2.3b. There are more complex

topologies whose output can have more than three values, and they fall into the category of multilevel inverters.

2.2.1.1 Voltage-Sourced Inverter

A typical voltage-sourced inverter, VSI, uses relative phase control to generate a three-level output. VSI controls are commonly used for H-bridge inverters and rely on the fact that the duty ratio of the switches is 50% [12]. This means that each switch is on for half of the period and off for half of the period. This ensures that there are no DC components in the output.

The VSI staggers when each switch is connected so that the output is zero volts during part of the cycle. For the H-bridge inverter topology, a non-zero voltage potential exists across the output terminals only when both switches in the diagonal pair (1,1 and 2,2 or 1,2 and 2,1 in Figure 2.3a) are closed. VSI delays the time that these switches close relative to on another, so that the output voltage is zero for a specific amount of time. The delay is called the displacement angle and is represented by a lowercase delta, δ. The value of the displacement angle influences the shape of the output waveform. If no delay occurs (δ=0) then the output is a square wave. However, if a delay exists, then the output voltage becomes a quasi-square wave similar to the one shown in Figure 2.3b [12].

There are several advantages that justify using the VSI control technique. VSI switches only operate once per cycle putting them into the category of low frequency switching. Other strategies, such as pulse-width modulation, (PWM) induce switching over a thousand times per cycle and are considered to be high-frequency switching. The act of switching consumes power, so the VSI inherently uses less power than PWM and other high frequency switching techniques. The PWM technique produces distortion at higher frequencies, so PWM inverters mandate different design criteria for their output filters (and typically require input filters as well) than VSI inverters [12]. Although there are often less harmonics in VSI inverters, these harmonics occur at

low frequencies – near the fundamental frequency – which can make filtering more difficult and require larger inductors.

The quasi-square wave produced by the VSI bears a closer resemblance to a sinusoid than a normal square wave. Both waveforms contain a number of harmonic components; however, the quasi-square wave will have less harmonic distortion than a square wave and produces a higher quality output. One key strategy behind the design of many inverters is to create an output that is as close as possible to a purely sinusoidal wave. Multilevel inverters are one such classification of inverters that with this goal in mind.

2.2.1.2 Multilevel Inverters

Increasing the number of levels in a waveform generally improves the quality of the waveform. Adding levels reduces the step size, which has been shown to reduce harmonic distortion [13]. Many researchers have developed new topologies that produce output waveforms that contain more than three levels. These inverters are lumped into a category called multilevel inverters. Such inverters have received significant attention in recent years because they operate with high efficiency, work particularly well in low, medium and high power systems, and can be readily applied to technology dealing with renewable energy sources, particularly solar [14].

Low-power systems (<10kW) that demand high efficiency inverters have recently seen an increasing presence of multilevel inverters instead of the PWM inverters previously used for these applications [15]. Multilevel inverter topologies are particularly attractive for use with renewable energy sources due to the nature of the physical arrangement and the level of power produced [16]. When connecting PV systems to the grid, multilevel inverters offer several advantages that include the ability to maximize power drawn from independently operating PV arrays and to reduce the filtering requirements of the output voltage [17].

The neutral-point clamped, NPC, topology is a multilevel inverter topology that first received attention in 1979 [18]. When multilevel inverters regained popularity in the early 1990's, the NPC topology gave rise to what is commonly referred to as the diode-clamped inverter. The flying capacitor is another multilevel inverter that is similar to the diode-clamped topology. These models are fed by a single DC voltage source, and have multiple capacitors, sometimes called dc-link capacitors, connected across that input. The capacitors provide intermediate voltage levels such that the output voltage can take one of several values that are some fraction of the input voltage.

Voltage imbalance constitutes a significant drawback associated with the diode-clamped and flying capacitor topologies. The flow of current through the DC-link capacitors will change the voltage potentials across them. This effect often leads to unequal voltages from one capacitor to the next creating an imbalance. This issue limits diode-clamped inverters to three levels in practical applications [16]. The flying capacitor inverter is not as limited by this because it can implement some voltage balancing capabilities in its control strategy; however, voltage imbalance still constitutes a significant obstacle to overcome for this topology [19, 20]. The diode-clamped and flying capacitor topologies also expose some of their circuit elements to severe reverse recovery stress, moderate voltage stress and parasitic resonance between capacitors [21]. Additional topologies exist that avoid voltage balancing issues altogether. One such topology is the cascaded H-bridge.

2.2.1.3 Cascaded H-Bridge Inverter

The cascaded H-bridge inverter is fed by multiple independent DC voltage sources. Voltage balancing is not an issue because the dc-link capacitors are not present. This topology was widely researched for use with renewable sources such as fuel cells, biomass and solar in the 1990's and is commonly used with renewable energy systems today [22]. Using multiple voltage

sources makes this inverter ideal for use with renewable and clean burning energy sources – including solar, fuel cells and biomass – which require a large number of independent systems to harvest energy and then combine their outputs to produce a single, sufficiently large output [22]. These independent systems often produce power at different levels because the conditions to which they are exposed vary from one system to the next. The cascaded H-bridge topology allows an inverter to extract the maximum amount of power from each system before conglomerating all the energy into a single output.

The cascaded H-bridge topology, also referred to as the series full-bridge topology or any variation between the two, is depicted in Figure 2.4. This topology receives its name from the fact that a full-bridge inverter, shown in Figure 2.3a, is connected to each DC voltage input. The outputs of each inverter are connected in series so that the inverter's output is the sum of their collective outputs. The output of a single H-bridge inverter can be one of three levels: 0, V_{dc}, or $-V_{dc}$. If all DC input voltages are the same, then the output waveform will have 2n + 1 levels, where n is the number of DC voltage inputs.

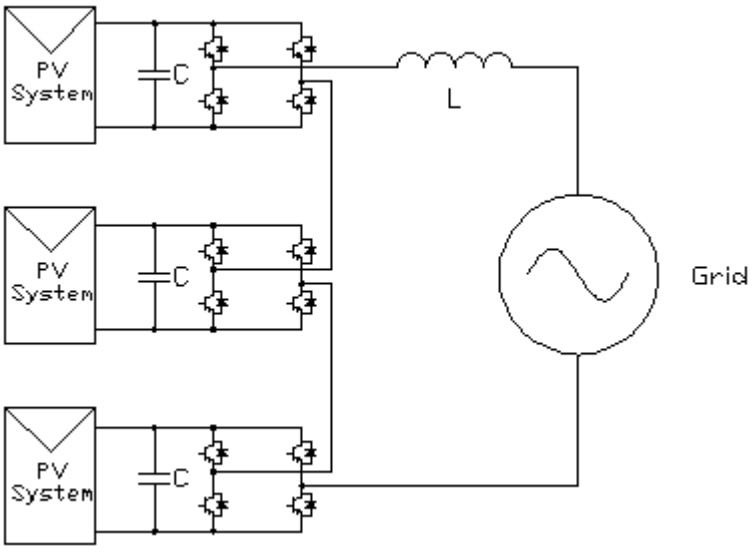

Figure 2.4: A seven-level cascaded H-bridge inverter connecting PV modules to the grid

This inverter topology is modular in nature, which presents several advantages over other topologies. The modular component includes the DC input and the full-bridge inverter. This modular nature could lead to implanting the inverter into the PV panel itself, which would simplify installation of the entire system and could reduce manufacturing costs. Additional modules can be easily added or removed from the entire system, allowing this inverter to be highly adaptable to different installation constraints. Furthermore, this modular input allows MPPT to be performed specifically for the input PV system, which ensures that the component is extracting maximum power from each PV system.

The cascaded H-bridge inverter has the ability to add levels to its output waveform without increasing the number of circuit elements. Simply by having different voltage levels for each of the DC inputs, the inverter can increase the number of voltage levels in its output waveform. For example, looking at Figure 2.4, when each DC input has a value of V_{in}, the output can take values between $-2V_{in}$ and $2V_{in}$, stepping in multiples of V_{in}. If the top DC input has a value of $2V_{in}$ and the bottom DC input has a value of V_{in}, then the output waveform can range from $-3V_{in}$ to $3V_{in}$, in multiples of V_{in}. Thus by having DC sources that produce voltage at different levels, the output voltage changes from a 5-level waveform to a 7-level waveform. In situations where the magnitude of the DC input voltage can be controlled, the cascaded H-bridge inverter has the ability to improve the power quality of its output waveform without increasing the number of circuit elements.

One obvious benefit of this inverter over other topologies is that the Cascaded H-bridge inverter has fewer components. This can lead to decreased cost, size and weight of the inverter, which can be highly advantageous in certain scenarios. Additional topologies have been suggested to further reduce the number of circuit elements required.

2.2.1.4 Reversing Voltage Inverter

One variation of the cascaded H-bridge inverter is capable of producing the same number of levels in the output waveform as its full-bridge counterpart but contains fewer components. Instead of a full-bridge inverter connected to each input source, a pair of switches is used to include or bypass that input. These pairs of switches are series connected such that this portion of the inverter is capable of producing a stepped, positive half-wave that is similar in nature to a rectified stepped full-wave. This half wave is passed through an H-bridge inverter that reverses the polarity periodically to produce a stepped full-wave across the output terminals. This topology is referred to as Reversing Voltage (RV). The circuit and the output associated with this topology are depicted in Figure 2.5.

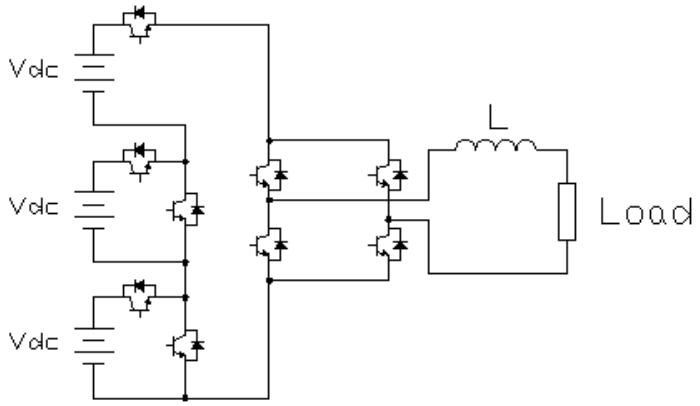

Figure 2.5: The seven-level reversing voltage topology

A reversing voltage inverter requires fewer circuit elements than other inverters capable of producing multilevel output waveforms. Voltage balancing is not an issue because it does not contain dc-link capacitors. As a result, the topology is not limited to a three-level output waveform. The control strategy for the reversing voltage inverter is less complicated than other inverters, and the topology is more reliable [23].

The topology implemented in the reversing voltage inverter has been a topic of research since 1994, [24] but it has only been applied to a small number of situations [25]. In its early applications, this topology was employed to increase the number of output voltage levels in order to improve the quality of the output waveform. Following the strategy described for the cascaded H-bridge inverter, the DC input voltages were designed to be unequal to increase the number of levels in the output [26]. More recently, since 2008, the topology been discussed for use in medium to high-voltage situations, specifically flexible AC transmission systems [23]. With continued research, additional applications for which this inverter is uniquely capable of producing optimal results may be discovered. One such application may be a micro inverter for a grid-tied PV system.

Control schemes associated with the H-bridge inverter in this circuit have hitherto focused on high-frequency switching techniques. It is argued that this switching strategy reduces the harmonics in the output waveform and improves efficiency. It has been proposed that low-frequency switching is possible with this topology, [27] although this option has not been pursued previously.

Many different multilevel inverter topologies exist. A large number of these are variations or combinations of the topologies hitherto described. While each topology presents unique advantages, the basic principles of operation are no different, so the details of these models do not provide any new knowledge relative to inverter topology or operation. Some topologies use transformers. Benefits of transformers include physical isolation of the circuit, the ability to step up the voltage level, and effectively increasing the apparent number of voltage sources, among other things. The variations in topologies including transformers are practically endless. Because this paper proposes a transformerless inverter, a discussion of inverters that include transformers is out of its scope.

The diode-clamped, flying capacitor and cascaded H-bridge topologies previously discussed represent the three most common inverter topologies currently in use. These topologies simply reflect ways to convert voltage from DC to AC. Some of the topologies discussed thus far have been applied specifically to connect PV systems to the utility grid. These inverters have more responsibilities than simple DC to AC conversion. They are designed with those goals in mind and often incorporate additional circuit components.

2.2.2 Voltage Gain Strategies

Inverters specifically designed to connect PV systems to the utility grid have three main tasks to perform: convert DC to AC, increase the voltage level and produce an output that meets grid specifications. These inverters employ myriad methods to complete the three objectives. The specific design and control scheme are often chosen based upon subtle differences between topologies and strategies that are best suited for the application. Please note that moving forward the paper will use the term inverter to designate the entire system that is used to connect the PV array to the utility grid, not simply the portion that converts DC to AC that was described in the previous section.

The voltage produced by an individual PV cell is too low to serve any useful purpose; however, inverter topologies are designed to compensate for this fact and still produce an output voltage at the desired level. A typical PV cell that occupies 0.01 m^2 is capable of producing an output of approximately 0.5 V [28]. It is common for a PV panel to consist of 36-72 PV cells connected in series in an attempt to have an individual panel that produces voltage at a useful level [29]. While the voltage level generated by such a panel, generally less than 50 V in an open circuit condition, is useful for some applications, it is usually too low to allow for connection to a utility grid. One solution is to group multiple panels together in various configurations to produce an array of panels. The voltage produced by the array is sufficiently large that it can be inverted

and connected directly to the grid. Other solutions boost the voltage produced by an individual panel to the proper voltage level.

It should be noted that connecting cells in series has several unintended consequences. According to KCL, elements connected in series will have the same current flowing through each element. If one element fails, then the flow of current is limited by the defective element. With respect to PV cells, if a single cell is shaded, then its MPP will exist at lower current and voltage levels than those cells that are not shaded. The MPP current of that cell would establish the current that flows through every cell. This effect will result in a drastic reduction in a panel's output [30]. To prevent this effect, most panels have diodes connected across a cell's output terminals to allow another path for the current when it cannot flow through that cell. These diodes are called bypass diodes, and they allow the panel's output power to not be significantly reduced by any single cell. They have the additional benefit of protecting the cells as well because they prevent the cells from being subject to a destructive reverse voltage [31].

2.2.2.1 Single-stage Versus Two-stage Topologies

One common technique that allows inverters to produce desirable output levels is to simply increase the voltage produced by an individual panel or array. Many inverter systems use a DC-DC boost converter, Figure 2.6a, to step up the DC voltage produced by the PV panel and then use an H-bridge inverter to convert that higher DC voltage to an AC voltage. These inverters are considered two-stage inverter topologies, Figure 2.6a.

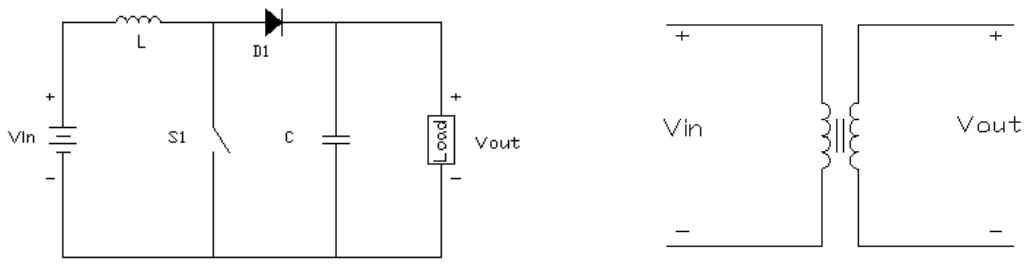

(a) A boost Converter (b) A transformer

Figure 2.6: Circuit elements required to increase an (a) DC voltage or (b) AC voltage

Two-stage topologies have more circuit elements than single-stage topologies, most notably possessing an additional switch. The energy consumed by the switch in the boost inverter often results in a two-stage topology consuming more power than its single stage counterpart. Having an additional switch to control increases the complexity of the controls. In some cases this is desired, as it allows more flexibility in control strategy. However, additional complexity and more circuit elements will increase the system's cost and reduce the system's reliability [32].

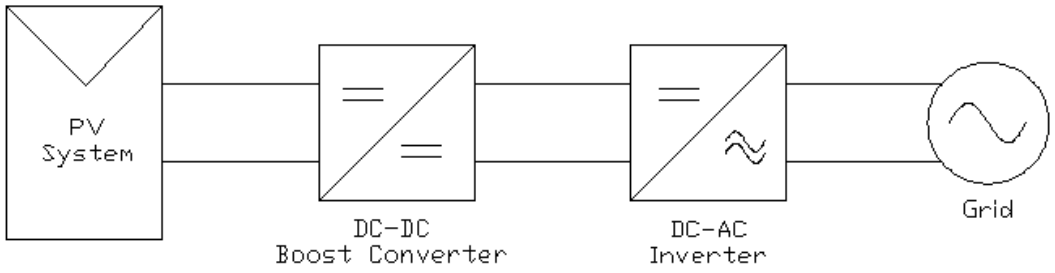

(a)

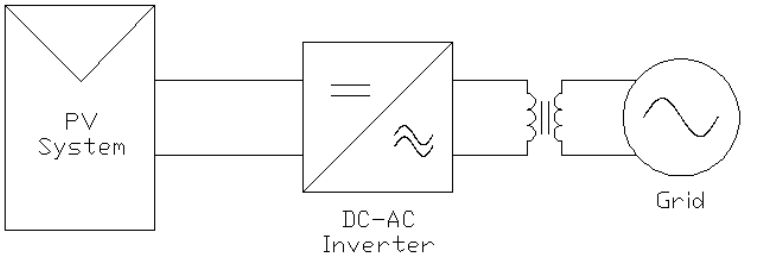

(b)

Figure 2.7: (a) Two-stage and (b) single stage voltage boosting inverters

Single-stage topologies differ from two-stage topologies in that there exists only a single inverter circuit in the system to convert the DC input into an AC output. Analogous to the DC-DC boost converter, a single-stage topology may introduce a step up transformer on the output side of the inverter to boost the AC voltage to the required level, Figure 2.7b. The transformer is often preferable to the boost converter because it provides physical isolation of the two circuits and prevents loss associated with leakage currents [26]. Being a passive element with no moving parts, the transformer does not need to be controlled and is less likely to fail unexpectedly.

Certain single-stage topologies exist that do not require a transformer to step up the AC voltage level. These inverter topologies feed off of an input voltage that is high enough to allow the inverter to produce an adequately large output voltage. These types of inverters are classified

into several categories based upon the configuration of the PV arrays with respect to the inverters. The most common categories are central-inverters, string-inverters and micro inverters.

2.2.2.2 Central, String and Micro Inverters

Inverters that connect PV systems to the utility grid are categorized into one of three categories: central, string or micro. Rough schematics of these layouts in single-stage topologies are shown in Figure 2.8. These inverters employ different methods to connect PV systems to the utility grid, and each has its own strengths and weaknesses.

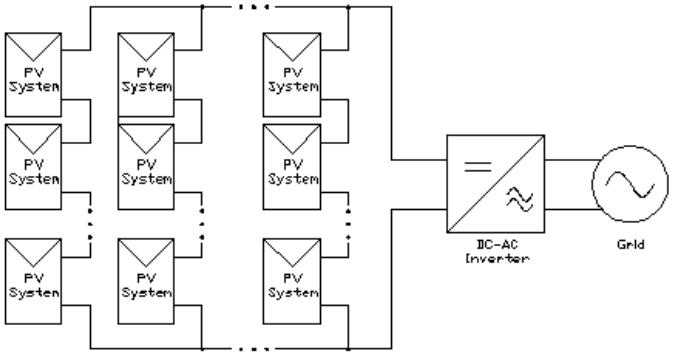

(a)

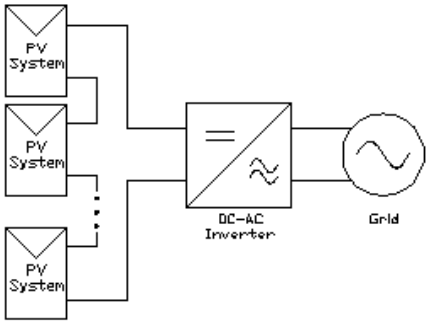

(b)

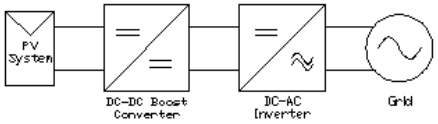

(c)

Figure 2.8: PV array configurations for (a) centralized, (b) string and (c) micro inverters

Central inverters are the traditional type of PV inverter. These inverters typically produce power at levels greater than or equal to 10 kW [33]. Central inverters connect many PV panels in

series to generate a high voltage potential between busses. They connect multiple strings of panels in parallel to ensure that the voltage potential seen at the inverter's input remains constant. A single inverter is then used to convert that voltage to AC. MPPT occurs once for the entire array of PV panels. The voltage across each string of panels is equal, and all the panels in a string have the same current flowing through them.

Central inverters are particularly attractive for large-scale solar applications, such as solar farms. The cost per unit of the entire system is often reduced through scalability factors. These systems are usually installed in large, flat, open areas and typically employ centralized MPPT. Although this layout exposes panels to nearly identical levels of solar irradiation, the little mismatch that does exist limits the amount of power that can be extracted from the whole system as a result of the centralized MPPT. Due to this fact, central inverters often have higher relative amounts of power losses than string and micro inverters [34].

String inverters typically generate between 0.5 and 1 kW of power. From the name, it can be inferred that these inverters use a string of PV panels connected in series as their input DC voltage. MPPT is performed for an individual string instead of for all the strings combined, as was the case for the central inverter. This feature allows string inverters to extract more power from their PV panels than comparable central inverters because MPPT occurs for each individual string so the number of panels that can hinder the performance of each string is significantly reduced. Similar to the case where individual PV cells are connected in series, as described above, when one panel in a string is shaded, the power output of the entire string is greatly reduced [35]. This logically creates a demand for micro inverters, which will be discussed momentarily.

In some applications, like Figure 2.8b, the string of PV panels in the string inverter typically produce a sufficiently high voltage so that a voltage boost is unnecessary for connection to the

grid. This application is particularly appealing as it allows for flexibility in array configurations and added reliability when multiple strings work in parallel.

In other cases, boost converters are needed to boost the DC voltage produced by each string before feeding a centralized inverter. These are often referred to as multi-string inverters and are depicted in Figure 2.9. Like string inverters, the multi-string inverter performs MPPT for each string of PV panels, and is able to extract more energy per string than a comparable centralized inverter. Parallel operation of strings is still possible, and the PV system can easily be enlarged as a result of the boost converters. Unfortunately, the single point of failure between the inverter and grid eliminates the redundancy and reliability that exists with the string inverter.

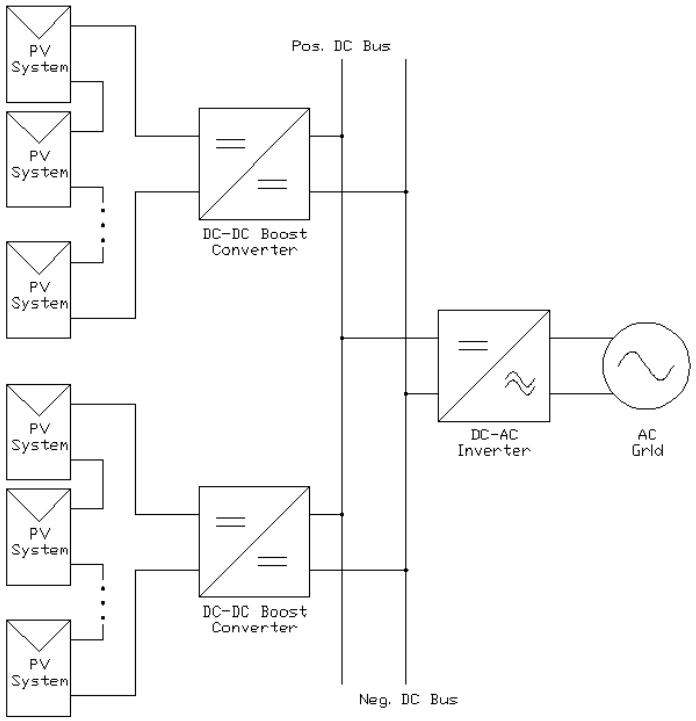

Figure 2.9: Multi-string inverter

Micro inverters, Figure 2.8c, often connect individual PV panels to the utility grid; they typically generate around 300 W of power or less [33]. They are intended to be incorporated into

the panel itself, and for this reason are sometimes referred to as AC Modules. The modular concept consists of the combined PV panel and built-in micro inverter, which allows each panel to have “plug and play” capabilities. The installation process becomes drastically simplified as panels can be easily inserted or removed to meet the needs of a specific application.

While the upfront cost per watt of an AC module is often higher than that of a string or centralized inverter, the ease of installation and higher level of power extraction make it much more attractive and cost effective in smaller installations. MPPT is performed for each individual panel with a micro-inverter. This completely eliminates the voltage mismatch between PV panels that exists in centralized inverters and, to a lesser extent, string inverters. More power is extracted from each panel as a result.

An additional benefit associated with the micro inverter manifests itself when multiple modules are connected to the grid. The redundant nature of units individually connected to the grid provides reliability. Similar to the case of the string and multi-string inverters, a single micro inverter or PV system can fail, but the rest of the micro inverters will continue to operate normally. Thus, in the case of failure of a single unit, the total power delivered to the grid will decrease, but it will not be reduced completely to zero.

2.2.3 Harmonics

One of the main roles of a grid-tied inverter is supplying power to the grid. The inverter must generate a high quality output waveform to improve the performance of the overall system and meet the interconnection requirements of the grid. Interconnection requirements often pertain to voltage magnitude, voltage notching, frequency, power factor and distortion. The latter can be the most difficult requirement to meet and is of utmost importance to this paper. In some cases, this standard is defined in terms of the total harmonic distortion, THD, present in the

waveform. THD quantifies distortion based upon the presence of different Fourier components in the waveform.

2.2.3.1 The Fourier Series

Any reasonably periodic waveform can be expressed as the summation of sine waves and cosine waves [12]. This mathematical description of the waveform is known as the Fourier series and is expressed in the following equation.

$$f(t) = a_0 + \sum_{n=0}^{\infty} (a_n \cos(n\omega t) + b_n \sin(n\omega t)) \quad (1)$$

In (1), omega, ω, represents the angular frequency of the waveform. It is directly proportional to the frequency, f, and inversely proportional to the period, T. The Fourier components are part of the Fourier series, and their integer multiples (n=1, 2,…) are typically referred to as harmonics. The Fourier components are defined as:

$$a_n = \frac{2}{T} \int_{\tau}^{\tau+T} f(t) \cos(nwt) dt \quad (2)$$

$$b_n = \frac{2}{T} \int_{\tau}^{\tau+T} f(t) \sin(nwt)\, dt \quad (3)$$

Equation (1) can be rewritten in an alternative form by introducing several different variables that represent combined terms.

$$f(t) = \sum_{n=0}^{\infty} c_n \cos(n\omega t + \theta_n) \quad (4)$$

Of chief concern is the frequency at which these waves oscillate. As is the case in AC systems, both voltage and current oscillate. Average power flow occurs only when the current

and voltage components have matching frequencies [12]. The same concept can be extrapolated to the inverter in that only power whose frequency matches the load supplies power to the load. The wanted component in the output waveform is the component whose frequency matches that of the desired load being served. The wanted component in this case is the fundamental component and includes the harmonic components associated with n=1, assuming the frequency associated with omega is equal to the frequency of the load. The unwanted components are all the other harmonic components present in the waveform.

The a_0 term in equation (1) constitutes the DC component in the waveform. When supplying power to an AC load, one must virtually eliminate this DC component to avoid damaging equipment and circuit elements designed exclusively for AC. As has been discussed previously, inverter controls are strategically employed to eliminate any DC component in the output waveform.

2.2.3.2 Total Harmonic Distortion

There are several metrics used to quantify the presence of unwanted components in a given signal. Total harmonic distortion (THD) is one such metric that is a ratio of the RMS values of the unwanted components and the fundamental component. The larger a waveform's THD, the more unwanted components are present in the signal. This is commonly written in one of two ways.

$$\text{THD} = 100 * \sqrt{\frac{(f_{RMS})^2 - \left(f_{RMS,fund}\right)^2}{\left(f_{RMS,fund}\right)^2}} \tag{5}$$

$$\text{THD} = 100 * \sqrt{\frac{\sum_{n=2}^{\infty}(f_n)^2}{(f_1)^2}} \tag{6}$$

IEE Standard 519-1992 identifies distortion limits for Transmission and Generation systems. This standard lists different distortion limits based upon the size of the load with respect to the size of the power system to which the load is connected [36]. For the purposes of this paper, the utility grid constitutes the power system, and the inverter's output constitutes the load. To calculate a system's THD, one would use Equation (5) with respect to the current Systems would use Equation (5) to calculate the THD present in the current waveform, where $f_1=I_L$.

The IEEE standard refers to extremely high voltage levels relative to the residential utility-grid voltage levels addressed in this paper. It is common for applications involving lower voltage and power levels to calculate the THD with respect to the rated fundamental current of the system to avoid over-penalizing these low-load applications The THD in the output current from the proposed inverter will be calculated based upon a rated current. The calculated THD will be compared to the IEEE standard to assess the performance of the inverter.

3 Methodology

This paper proposes a single-phase inverter topology that serves as the interface between a system of PV modules and the utility grid. The inverter employs a topology similar to that of the reversing voltage (RV) inverter to extract power from several PV modules operating independently of one another. MPPT is performed separately for each PV module. The proposed inverter seemingly falls into the category of micro inverters for its modularity and the high level of granularity that it performs MPPT; however, the levels of voltage and power produced by the inverter are slightly higher than those produced by a typical micro inverter.

The proposed topology, Figure 3.1, produces a multilevel output waveform in the same manner as the RV topology described in section 2.2.1.6. There exists a pair of switches associated with each input. These pairs are strategically operated to change the number of DC voltage inputs that are connected in series over time. This action produces a stepped half-wave, which is also called a positive stepped waveform or a rectified stepped waveform. The stepped half-wave is fed through an H-bridge inverter that reverses the polarity of the waveform periodically to produce a nearly sinusoidal output waveform.

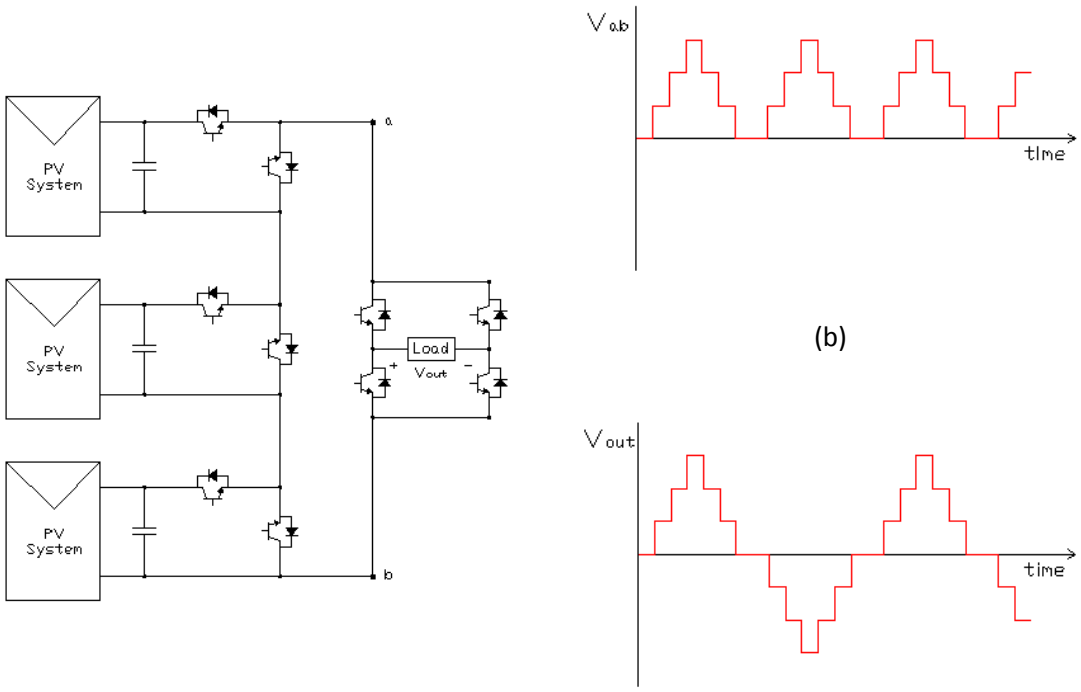

Figure 3.1: A seven-level version of the proposed inverter topology (a) and the stepped half-wave (b) and output (c) it produces

The proposed inverter outperforms the RV topology and applies to different systems than the RV topology because of the control scheme employed. The proposed control scheme allows each DC input voltage to exist at different, not necessarily evenly incremented, levels and is able to respond to changes in input voltage levels. This enables the topology to use independent PV modules as the DC power sources. Furthermore, the control scheme uses low-frequency switching to reduce switching loss and improve the efficiency of the inverter.

The inverter proposed in this paper capitalizes on the advantages associated with the RV topology as a means to reduce the number of components in the inverter and improve its performance relative to other grid-tied PV inverters. Capacitor balancing issues do not exist within this topology because the inputs function independently of one another. As a result, the number

of levels in the output waveform is only limited by the number of input sources. This topology can accommodate enough input sources so that no additional voltage gain is necessary. As such, the inverter does not need a DC-DC boost stage or a transformer, which simplifies the design and control of the inverter.

It is easy to increase the number of inputs with the proposed topology, and it is desirable to have a larger number of inputs. Each input provides two additional levels to the output voltage and increases the quality of the waveform. Having more inputs reduces the number of PV cells that are connected in series. As a result, MPPT can be performed at a more granular level to reduce the negative effects of shading and increase the efficiency of the system. One major drawback associated with adding inputs is that two switches must be added for every additional input. The benefits described above must be weighed against the power consumed by the added switches to find the optimal number of inputs for a given situation.

The modular nature of inputs associated with this topology improves the ease that additional inputs can be added. Each input has an associated capacitor and pair of switches. These can potentially be built onto the back of the PV panels, or possibly even the PV cells, at the manufacturing stage. This would make adding additional inputs extremely easy and lend the topology to be easily applied to a wide range of physical applications.

A computer model of the proposed inverter is developed with the Matlab software in the Simulink program to demonstrate the capabilities of the proposed system. This model includes blocks that simulate the performance of PV panels, perform MPPT for the PV panels, implement the desired control scheme and simulate the interconnection with the grid. A computer model of a comparable inverter capable of interfacing with the same PV system but using a VSI control technique has been created for comparison purposes.

3.1 Computer Model of the PV System

A simple mathematical model of a PV cell is introduced whose output power is dependent upon solar irradiance. This model is implemented in the Matlab program Simulink to simulate the performance of a cell. The Simulink model of a single cell is adjusted so that the model simulates the performance of an entire PV panel. The output produced by this computer model is shown to match the output of a real PV panel, demonstrating the validity of the Simulink model. The model is further adjusted to emulate multiple panels in series so that the output voltage is large enough to allow for grid connectivity without need of any type of voltage gain. Finally, the model is tweaked to simulate the performance of multiple PV modules operating independently whose collective output voltage is sufficiently high to support a connection with a utility grid.

3.1.1 Electrical Equivalent Model of a PV Cell

For the purposes of this paper, a mathematical model of a PV cell is required to simulate the output of a real PV system. The model must have the ability to produce representative results under different conditions to demonstrate the effectiveness of the inverter. There exist many complicated models of PV systems that take into account thermal and solar conditions to which PV systems are exposed. While these models more accurately simulate the performance of specific PV modules, this level of detail is unnecessary for the purposes of this paper. A simplified model is created in Simulink that depends solely upon a single variable: solar irradiance. Despite this simplification, the model adequately simulates the performance of a real PV panel.

A photovoltaic cell can be modeled by the electrical circuit shown in Figure 3.2. The two most important components in the model are the ideal current source and the ideal diode, which are connected in parallel. This model includes two resistors, one connected in parallel with the current source and the other in series with the output. The terminal points A and B represent the output of the PV cell.

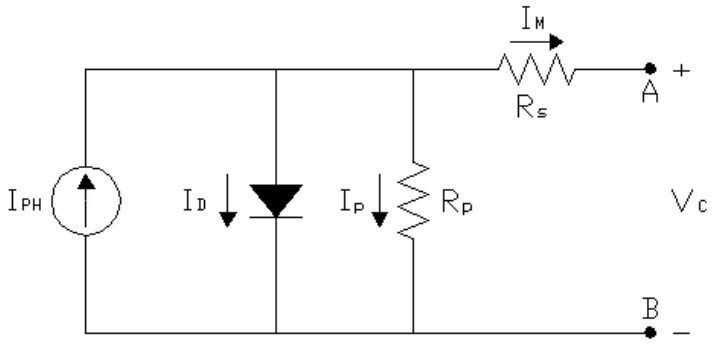

Figure 3.2: An electrical circuit used to model a PV cell.

The current source represents the electricity produced by the photovoltaic cell when illuminated. The parallel diode captures the unique and highly important nature of the P-N junction. The shunt resistance, R_P, accounts for losses associated with a leakage current that appears when cells are connected in parallel. The series resistance, R_S, accounts for losses in the path of the current flow, such as the inherent resistance in wires [37].

Adding a second diode in parallel allows the electrical model to better simulate the output of a real PV cell, but doing this drastically increases the complexity of the mathematical model [38]. Instead of adding another diode, one can adjust the Shockley diode equation to incorporate an ideality factor and accomplish the same goal [39]. It is shown that the ideality factor provides a level of compensation that allows the single diode model to more accurately match the output of a real cell without unnecessarily complicating the mathematical model. This ideality factor will be discussed in more depth as the mathematical model of the PV cell is developed below.

Applying Kirchhoff's Current Law (KCL) to the circuit in Figure 3.2 relates the currents flowing through each circuit element.

$$0 = I_{PH} - I_D - I_P - I_M \tag{7}$$

The current generated by the absorbed light at the P-N junction level is called the photon current and is represented by the term I_{PH}. This current is highly dependent on the environmental

conditions, particularly sunlight and heat, to which the junction is exposed. An estimated value of the current can be calculated according to Equation (8) [40].

$$I_{PH} = I_{sc,ref} \frac{G}{G_{ref}} \left(1 + \Delta I_{sc}\left(T - T_{ref}\right)\right) \quad (8)$$

$I_{SC,ref}$ is the short circuit current under STC, G_{ref} and T_{ref}. These values can be found on most data sheets provided by the manufacturer of the PV panel. The solar irradiance of the sunlight striking the PV cell is G, and the temperature of the cell is included in the equation as the variable T. The term ΔI_{SC} is a correction factor used to adjust for the temperature deviation from STC. This correction factor is typically included on a manufacturer's data sheet as well. This model does not take into account the effects of temperature, so the correction factor can be neglected.

The current flowing through the diode, I_D, can be modeled by Shockley's diode equation. The flow of current is highly dependent upon the semiconductor material, doping levels, and junction temperature [41]. Shockley's equation simplifies the complex relationship to closely approximate the value of the current based upon the voltage across the junction, V_D, and the junction temperature, T. The equation contains several constants, such as the elementary charge, q = 1.602×10^{-19} C, and Boltzmann's Constant, k = 1.381×10^{-23} J/K.

$$I_D = I_{sat}\left(e^{\left(\frac{qV_D}{N_s nkT}\right)} - 1\right) \quad (9)$$

The equation has an ideality factor, n, which is sometimes referred to as the emission coefficient. The inclusion of this variable coefficient allows the equation to more accurately model the behavior of real diodes that may have some imperfections at the junction level due to manufacturing difficulties. The ideality factor ranges from 1 to 2, and when it equals 1 the equation becomes Shockley's ideal diode equation. In using the equation for modeling PV cells, the ideality coefficient is never one in order to account for the absence of a second diode. In many

applications the ideality factor is determined experimentally to adjust the mathematical model so it accurately simulates the performance of a specific PV module [20].

The coefficient, N_s, is included in the equation when it is applied to PV systems, in accordance with industry standards. This variable identifies the number of cells connected in series for a given panel. This value is generally listed on the data sheet.

The reverse saturation current, I_{sat}, is an important component of Equation (9). This variable is an innate aspect in the P-N junction and quantifies the current associated with the minority current carriers present in the semiconductor material. The reverse saturation current can be calculated if one has knowledge of doping levels, physical dimensions, and certain physical properties associated with the semiconductor comprising the junction [41]. For the purposes of modeling a PV cell, such detailed information is generally not readily available, so many methods have been recommended that estimate values for the saturation current using values given on the manufacturer's data sheet. It is shown that Equation (9) produces a sufficiently accurate value for the saturation current [37], so this equation is used for the model being developed in this paper.

$$I_{sat} = \frac{I_{sc}}{\left(e^{\left(\frac{qV_D}{nkT}\right)} - 1\right)} \tag{10}$$

Returning to the electrical circuit in Figure 3.2, many models often neglect the shunt resistor. One reason for this is because the resistance of the shunt resistor can often be at least two orders of magnitude larger than the series resistance. Additionally, the effects of the shunt resistance only become noticeable when a significant number of cells are connected in parallel [38]. Generally PV cells are connected in series, so the series resistance has a much greater effect on the performance of the PV system. This paper does incorporate the shunt resistance and calculates rough approximations for both resistances based upon data sheet values [38].

$$R_P = \frac{100 \times V_{OC}}{I_{PH}} \times \left(1 + \Delta I_{sc}\left(T - T_{ref}\right)\right) \tag{11}$$

$$R_S = \frac{0.01 \times V_{OC}}{I_{PH}} \times \left(1 + \Delta I_{sc}\left(T - T_{ref}\right)\right) \tag{12}$$

Due to the unique relationship between current and voltage produced by a PV cell, this paper is interested in both the output voltage, V_C, and the output current, I_M, of the PV cell. It is beneficial to limit the mathematical equations describing the behavior of the electrical equivalent circuit to these two variables. Simple implementation of Ohm's Law in Equation (13) conveys the voltage drop across the diode in terms of these two variables.

$$V_D = V_C + R_S \times I_M \tag{13}$$

Equations (8), (9), and (13) can be substituted into Equation (7) to produce Equation (14). Equation (14) is the mathematical equation that describes the operation of the electrical circuit in Figure 3.2. Equation (14) has three dependent variables, (G, V_C, and I_M) while the rest of the variables can be found on a manufacturer's data sheet or using one of the several equations listed above. The solar irradiance, G, is an input parameter used to simulate different conditions and adjust the output power of the PV systems. The voltage across the cell's output terminals, V_C, and the current flowing out of the cell, I_M, depend upon the operation of the inverter.

$$\begin{aligned} f(G, I_M, V_c) = {} & \frac{G}{G_{ref}} \times I_{sc} - \frac{V_C}{R_P} - I_M \times \left(1 + \frac{R_S}{R_P}\right) - I_{sat}\left(e^{\left(\frac{q(V_C + R_S \times I_M)}{N_S nkT}\right)} - 1\right) \\ & = 0 \end{aligned} \tag{14}$$

Equation (14) is highly non-linear and cannot be solved analytically, so it must be solved numerically. The equation can be solved by assigning a value to the solar irradiance, G, and the output voltage, V_C, then using one of several techniques to approximate the output current, I_M. The computer program MATLAB has a function called *fsolve* that can calculate the current

corresponding to a specific voltage. One can also use Newton's method as another approach solving the equation.

$$x_{n+1} = x_n - \alpha \frac{f(x_n)}{f'(x_n)} \tag{15}$$

Newton's method employs an iterative process to find an approximate solution to a given function. The function must be defined with a single variable and written to equal zero. An initial value is estimated for the variable. Newton's method plugs this value into the function and calculates the result. It also calculates the derivative of the function for that value. The function and the derivative are compared to one another to calculate a new value for the variable that is closer to actual solution. This constitutes one step of the Newton method. It is represented in Equation (15) and the Simulink implementation is shown in Figure 3.3. Newton's method uses the derivative of Equation (14) taken with respect to current, so the derivative is presented in Equation (16).

$$f'(I_M) = \frac{\partial}{\partial I_M}[f(G, I_M, V_C)] = -\left(1 + \frac{R_S}{R_P}\right) - \frac{qR_S I_{sat}}{N_S nkT} e^{\frac{q(V_C + R_S I_M)}{N_S nkT}} \tag{16}$$

There exists a tradeoff between time and accuracy with Newton's method. As each Newton step pushes the results closer to the actual solution, it is clear that executing fewer iterations takes less time to perform but yields less accurate results. As such, the precision of the output is used to determine the number of Newton steps necessary to yield desirable outputs. By comparing the results of Newton's method to the *fsolve* command, five iterations of Newton's method provide sufficiently accurate results (<1 % difference). Tests show that Newton's method requires considerably less computation time than *fsolve*, 0.0022 s to 1.5853 s respectively. As a result, the model presented in this paper uses five Newton steps to approximate the solution to Equation (14) to save on computational power without sacrificing accuracy.

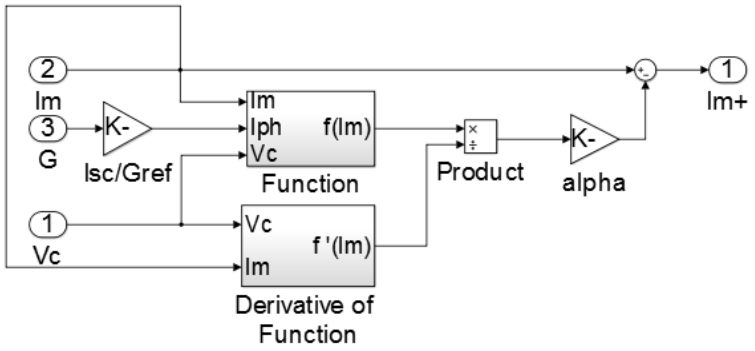

Figure 3.3: A single Newton step in the Simulink model

In this way, one can approximate a single operating point of the PV cell exposed to that level of solar irradiance. By assigning a different output voltage, the equation can be solved again to identify a second operating point of the PV cell. Solving the equation to find the corresponding output currents for many values of V_C that exist between 0 and V_{OC} allows one to create the I-V curve for that PV cell under a given level of solar irradiance.

The model now has the capabilities of simulating the performance of an individual PV cell. All that remains is finding values to plug into the above equations so the model can run. While any values can be selected in theory, it is desired that the Simulink model simulates the output of a real PV system. As such, the next step is choosing an actual PV panel to emulate so that the data sheet values associated with that template can be used to find values for coefficients in the previous equations.

3.1.2 Adjusting the Model to the Whole System

A Simulink model has been developed that can simulate the performance of a single PV cell under a given solar irradiance; however, this model must be adjusted to match the entire PV system that will be used with the proposed inverter. The model must first be scaled to simulate the output of a real PV panel to verify the accuracy and capabilities of the model. The model will

then be adjusted so that it is capable of mimicking the performance of independently operating PV systems that collectively produce a sufficiently high output voltage.

In general, PV panels are simply multiple cells connected in series, so adjusting the PV cell model is not terribly difficult. Specifically, Equation (9) contains a coefficient, N_S, in the calculation of the diode current that accounts for having multiple cells connected in series. Furthermore, the other variable coefficients scale proportionally to the number of cells in series due to the nature of the electrical circuit model of the PV cell. Specifically, the series and shunt resistances from one cell to the next are connected in series with one another and can be scaled accordingly. As such, the equations used to model the PV cell can model multiple cells in series by simply adjusting the coefficient N_S. As a result, values can be taken directly off the data sheet and plugged into the equations, and the Simulink model will accurately simulate the performance of the entire PV panel. The Simulink model that is developed in this paper is used to imitate the output of a real photovoltaic module (Grape Solar model: GS-P-280-Fab1). Values for various variables used in the model are extracted from the module's manufacturer's data sheet, which can be found in APPENDIX A.

Once the functionality of the Simulink model is proven, some slight changes are necessary to model a PV system that serves the exact purpose of this paper. To increase efficiency and power quality, the inverter introduced in this paper wishes to connect the PV system to the utility grid without the need for an additional voltage gain. To accomplish this task, the PV system must produce voltage at sufficiently high levels to allow for grid connectivity, namely greater than 170 V DC. A single panel does not produce voltage at this level, so multiple panels must be connected in series to produce voltage at the necessary level. Connecting panels in series essentially multiplies the number of individual PV cells connected in series. Luckily the same

approach as earlier can be taken to scale the model to simulate series connected panels: increasing the variable coefficients proportionately to the number of cells in series.

The Grape Solar PV panel produces 35.8 V DC when operating at its maximum power point under STC. As such, 5 modules can be connected in series to provide sufficiently high voltage to allow for grid connectivity without the need for additional voltage gain. The model is adjusted so that the number of cells connected in series, N_S, increased from 72 (one panel), to 360 (five panels). In real applications, more than 5 panels would be connected in series to ensure that sufficiently high voltage levels are produced because conditions are often less favorable than STC; however, this scenario is sufficient for demonstration purposes.

It is desirable that this large PV system be partitioned in a way so as to simulate the behavior of smaller independent PV modules whose collective output voltage is equivalent to that of the large PV model (5 panels connected in parallel). In the same way that the model is easily scaled to accommodate additional cells connected in series, the larger model can be easily partitioned to reflect fewer cells in series. The size of each smaller PV module could be as little as one cell operating independently or as large as 180 cells operating in series. The number of cells connected in series will determine the number and size of independently operating PV modules. There are 360 cells that are available in the larger PV system that must be included in the smaller PV modules to guarantee that the necessary output is produced.

Each smaller PV module will serves as an input DC source for the proposed inverter. It is desirable to have as many input sources as possible. As discussed earlier, increasing the number of levels in the inverter's output waveform generally improves the quality of the output waveform. Additionally, the performance of the PV system improves when fewer cells are connected in series because the effects of partial shading are reduced and MPPT can be performed at a higher granularity.

The proposed inverter uses four PV systems, N = 4, to serve as independent input DC voltage sources, as this is the minimum number of inputs that sufficiently demonstrate the capabilities of the inverter. By demonstrating the inverter works with four input sources, the performance reveals that the inverter is able to work with any number of input sources. The simulation uses the minimum number of inputs necessary in order to reduce the computational power and amount of time required to run simulations.

3.2 Maximum Power Point Tracking

In dynamic systems, myriad maximum power point tracking, MPPT, techniques exist to accurately track, in real time, the operating point that produces the most power. These techniques typically analyze the current and voltage that are produced by the PV system and adjust a specific parameter that causes the system to operate at a point closer to its MPP. These techniques are extremely effective in ensuring that the operating point closely follows the MPP.

The Simulink model of the PV systems discussed in this paper is not as complex as a real PV system. The model simply generates an output based on Equation (14). Looking at the equation, it is apparent that the I-V curve produced by the system can be determined if the level of solar irradiance is known. Complicated MPPT techniques are not needed for computer simulations involving the proposed inverter because the level of solar irradiance is given as an input value, as shown in the figure below.

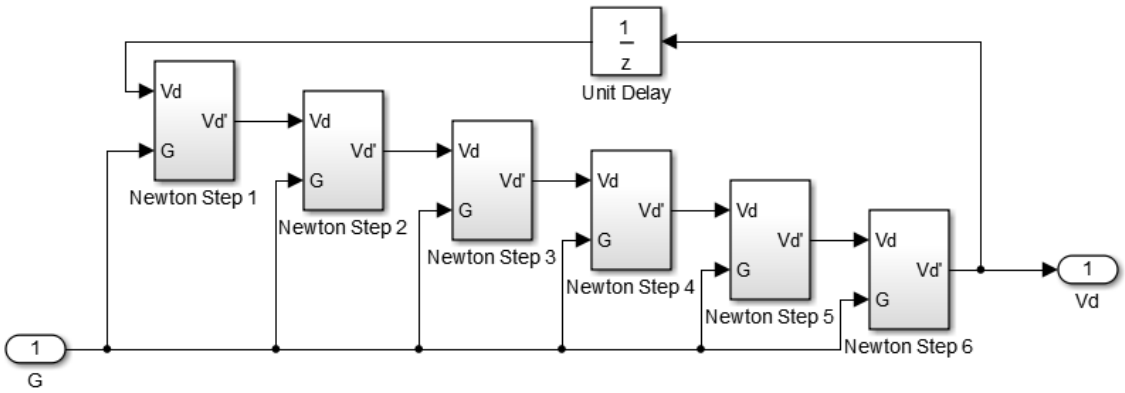

Figure 3.4: Using Newton's method to perform MPPT in Simulink model

MPPT in this paper is calculated exclusively using the solar irradiance. Equation (14) is modified using Ohm's Law, as implemented in Equation (13), to be a function of solar irradiance, G, the output current, I_M, and the voltage across the diode, V_D. This equation is rearranged so that the output current can be written using only the solar irradiance and voltage across the diode, as shown in Equation (17). Please note, that when performing MPPT, the solar irradiance will be known so it is considered a constant.

$$I_M = \frac{G}{G_{ref}} \times I_{sc} - \frac{V_D}{R_P} - -I_{sat}\left(e^{\left(\frac{qV_D}{N_s nkT}\right)} - 1\right) \tag{17}$$

The power delivered to the PV system is the product of the output current, I_M, and the voltage across the capacitor, V_C. This is written to exclude the term V_C, using Equation (13), as,

$$P(I_M, V_D) = I_M \times (V_D - R_s \times I_M) \tag{18}$$

This equation can be rewritten as a function of the unknown variable, V_D, by plugging Equation (17) into (18). Basic calculus indicates that a local maximum or minimum exists at a point on a function where the derivative is zero. To find the maximum power produced by the PV system for a given solar irradiance, one must take the derivative of Equation (18) and set it equal to zero.

Finding a value for V_D that solves Equation (19) will yield the value for V_D that corresponds to the MPP. The derivative is shown below.

$$\frac{\partial}{\partial V_D}[P(I_M, V_D)] = 0 \tag{19}$$

Newton's method is employed to solve for the unknown variable, V_D, in Equation (19). This requires taking the second derivative of Equation (18) with respect to V_D; however, that equation will not be shown. It requires six Newton steps to generate a reasonably accurate voltage across the diode associated with the MPP. The Simulink block calculating MPP is shown in Figure 3.4. The subsystem that performs a single Newton step is presented in Figure 3.5.

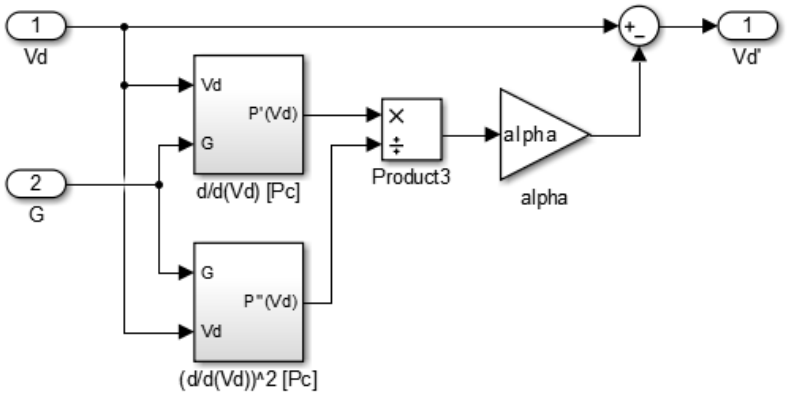

Figure 3.5: Simulink implementation of a single Newton step for MPPT

The value produced by the MPP block, V_D, can be plugged into Equation (17) and then (13) to yield the output current and output voltage of the PV system's MPP. These values are fed to the inverter's controller, which adjusts certain operating parameters of the inverter to push the PV systems towards the MPP.

3.3 Control Scheme

A single controller exists to monitor the performance of the inverter and orchestrate the operation of the switches in Figure 3.6. The control scheme is established with two goals in mind:

eliminate harmonic content in the output voltage waveform and deliver electricity to the grid at unity power factor. It is not possible to achieve both goals simultaneously because of certain physical restraints inherent in the topology. The control system employs a constrained optimization approach to coordinate the low frequency switching in a way that minimizes harmonic distortion and reactive power in the output.

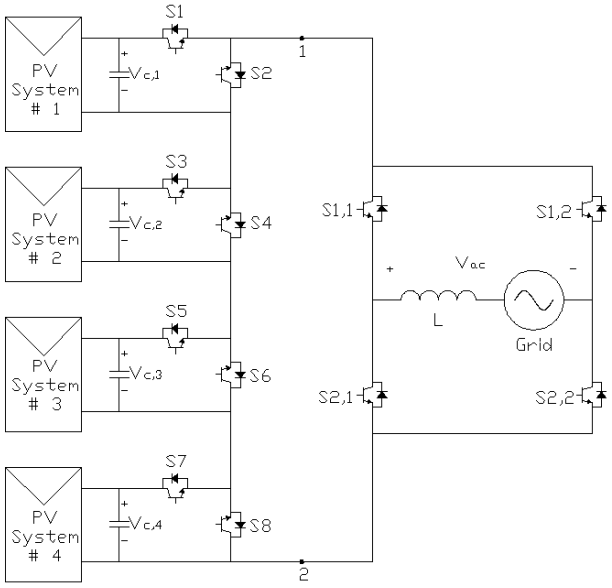

Figure 3.6: Topology of the proposed inverter

The control of the switching can be divided into two logical categories: sub-module switching and utility-level switching. Sub-module switching involves switches $S_1 – S_8$ in Figure 3.6 that are directly connected to the outputs of the PV modules. These switches determine the shape of the output voltage waveform and influence the power factor of the electricity supplied to the grid. Switches $S_{1,1} – S_{2,2}$ in Figure 3.6 are the utility-level switches. These periodically reverse the polarity of the voltage waveform to produce an AC voltage.

3.3.1 Sub-Module Switching

The sub-module switches control which input DC voltage sources contribute to the output voltage of the inverter. The voltage potential across terminals 1 and 2 in Figure 3.6 depends upon the number of inputs connected in series to the terminals. The controller changes the number of inputs to change the voltage potential across the terminals. Strategic coordination of the sub-module switches generates a stepped output waveform. The exact logic that determines when an input is connected depends upon the voltage levels of that input.

Each input has a pair of switches associated with it, for example S_1 and S_2 are associated with Input 1. The odd numbered switch connects the input in series with terminals 1 and 2 when closed. To simplify the explanation, the odd numbered switches will be the focus of the remaining discussion.

The state of the switches reveal if the inputs are connected or bypassed and thus can be used to describe the voltage potential across terminals 1 and 2. The switching function, q, indicates that a switch is open or closed by taking a value of 0 or 1, respectively. This paper will use q_i to describe the state of the odd switch associated with the *i*-th input. For example, $q_2 = 1$ reveals that S_3 is closed and input 2 is initially connected. The voltage potential seen across the output terminals 1-2 is labeled as v_{dc}. This equals to the sum of input voltages, $V_{C,i}$, that are connected in series at a given time. There are 4 independent PV systems, and thus N = 4 input DC voltage sources. Using this nomenclature, the voltage potential across terminals 1 and 2 can be expressed as a function of the phase angle of the grid voltage, θ_V, as shown in Equation (20).

$$v_{dc}(\theta_v) = \sum_{i=1}^{N} q_i(\theta_v)\, V_{c,i} \tag{20}$$

The value of the switching function can be identified with respect to the time that the switch opens. Specifically, the odd numbered switch associated with the *i*-th input is instructed to

close ($q_i \rightarrow 1$) when $\theta_V = \theta_{i,on}$ and open when $\theta_V = \theta_{i,off}$. Moreover, if a switch is open initially, $q_i(\theta_V=0) = 0$, the instruction to close will precede the instruction to open. If, however, the switch is closed at the beginning of the cycle, the order that the instructions are given will be reversed. The equation below captures this idea and defines the value of the switching function as a function of θ_V.

$$q_i(\theta_v) = \begin{cases} 1, & \theta_{i,on} < \theta_{i,off} \quad \cap \quad \theta_{i,on} \leq \theta_v \leq \theta_{i,off} \\ 1, & \theta_{i,off} < \theta_{i,on} \quad \cap \quad (\theta_v \leq \theta_{i,off} \quad \cup \quad \theta_v \geq \theta_{i,on}) \\ 0, & else \end{cases} \tag{21}$$

The control scheme is responsible for choosing when each input should be connected, so the controller assigns values to $\theta_{i,on}$ and $\theta_{i,off}$. These values dictate the shape and phase of the output waveform, which affect the THD and power factor. The voltage produced by each PV system plays a crucial role in determining when that input will be connected. The controller uses the input capacitor voltages to coordinate the sub-module switching in order to produce the optimal shape for the output voltage waveform. Optimizing the shape of the waveform minimizes THD in the output.

The periodic nature of v_{dc} enables the qualities of the waveform to be described mathematically. In a steady state situation, the voltage across each input capacitor will remain constant. It follows that the values of $\theta_{i,on}$ and $\theta_{i,off}$ will not change, so the close and open commands will be sent to each switch at the same time every half-cycle. In this way the function v_{dc} repeats itself and becomes periodic, as portrayed in Equation (22).

$$v_{dc}(\theta_v) = v_{dc}(\theta_v + \pi) \tag{22}$$

The H-bridge inverter reverses the polarity of v_{dc} every half cycle to simplify the mathematical analysis of the Fourier series. The strictly positive signal, v_{dc}, is transformed into an AC signal when it passes through the H-bridge. These different output waveforms are depicted in

Figure 3.1b and c. The Fourier series can now be used to quantify the harmonic content present in v_{dc}, which will be used to calculate optimal values for $\theta_{i,on}$ and $\theta_{i,off}$.

3.3.2 Calculating THD

The controller calculates THD in the output voltage waveform, v_{ac}. The output can be described in terms of v_{dc} as the H-bridge simply reverses the polarity of v_{dc}. Using Equation (20), the output voltage can be written simply as a function of the phase angle of the grid voltage, θ_V, and the input capacitor voltage, $V_{C,i}$.

$$v_{ac}(\theta_v) = \begin{cases} \sum_{i=1}^{N} q_i(\theta_v) V_{C,i}, & \theta_v \in [o, \pi] \\ -\sum_{i=1}^{N} q_i(\theta_v - \pi) V_{C,i}\,, & \theta_v \in [\pi, 2\pi] \end{cases} \tag{23}$$

The output waveform can also be described using the Fourier series as in the equation below. Note that the a_0 term in Equation (24) corresponds to the DC component in the waveform. Ideally this term will equal zero because there should be no DC component in the output AC waveform.

$$v_{ac}(\theta_v) = a_0 + \sum_{n=0}^{\infty} (a_n \cos(n\theta_v) + b_n \sin(n\theta_v)) \tag{24}$$

The fundamental component is an important aspect of the output waveform because it is used to calculate the THD in the signal. The fundamental includes all terms where n=1. The fundamental component of the output voltage is:

$$v_{ac,fund}(\theta_v) = a_1 \cos(\theta_v) + b_1 \sin(\theta_v) \tag{25}$$

The fundamental component of the output voltage contains the fundamental Fourier components, a_1 and b_1. These components are defined using Equation (2).

$$a_1 = \frac{1}{\pi}\int_0^{2\pi} v_{ac}(\theta_v)\cos(\theta_v)\,d\theta_v \tag{26}$$

$$b_1 = \frac{1}{\pi}\int_0^{2\pi} v_{ac}(\theta_v)\sin(\theta_v)\,d\theta_v \tag{27}$$

The interval 0-2π rad comprises a single period. Equation (23) shows that the waveform repeats itself, though with opposite polarity, twice in a single period. As such, the integral taken from 0-π rad will produce the same value as that taken from π-2π rad. Thus, Equations (26) and (27) can be rewritten to simplify the analysis. Only the fundamental Fourier component a_1 will be elaborated to demonstrate this point.

$$a_1 = \frac{2}{\pi}\int_0^{\pi}\sum_{i=1}^{N} q_i(\theta_v)V_{c,i}\cos(\theta_v)\,d\theta_v \tag{28}$$

The switching function will take a discrete value of zero or one. The expression for the fundamental Fourier components can be further simplified to only those intervals where the switching function takes a value of one. Such intervals can be expressed using the unknown variables $\theta_{i,on}$ and $\theta_{i,off}$. Care must be taken in this step as the order of $\theta_{i,on}$ and $\theta_{i,off}$ impacts the expression and solution.

$$a_1 = \frac{2}{\pi}\sum_{i=1}^{N} V_{c,i}\begin{cases}\displaystyle\int_{\theta_{i,on}}^{\theta_{i,off}}\cos(\theta_v)\,d\theta_v\,, & \theta_{i,on}\ \&<\ \theta_{i,off}\\ \displaystyle\int_0^{\theta_{i,off}}\cos(\theta_v)\,d\theta_v + \int_{\theta_{i,on}}^{\pi}\cos(\theta_v)\,d\theta_v\,, & \theta_{i,on}\ \&>\ \theta_{i,off}\end{cases} \tag{29}$$

Integrating these expressions yields:

$$a_1 = \frac{2}{\pi}\sum_{i=1}^{N} V_{c,i}\left(\sin\left(\theta_{i,off}\right) - \sin\left(\theta_{i,on}\right)\right) \tag{30}$$

$$b_1 = \frac{2}{\pi}\sum_{i=1}^{N} V_{c,i}\begin{cases}\cos(\theta_{i,on}) - \cos(\theta_{i,off}), & \theta_{i,on} \;\&< \; \theta_{i,off} \\ \cos(\theta_{i,on}) - \cos(\theta_{i,off}) + 2, & \theta_{i,on} \;\&> \; \theta_{i,off}\end{cases} \tag{31}$$

Equation (25) is an expression for the voltage produced with respect to the cosine of θ_V. Unfortunately, the proposed inverter model is designed with respect to the sine of θ_V, so the equation must be adjusted to reflect that. This adjustment can be made by introducing a phase shift of $\pi/2$ to the equation. Furthermore, all of the previous expressions have been written as a function of the phase angle of the inverter's output voltage. To ensure synchronization with the grid, it is necessary to write this expression as a function of the grid voltage. A phase shift exists between the grid voltage and the inverter voltage, reasons for which will be discussed shortly. As a result, the inverter's voltage will lead the grid voltage by the phase angle, ϕ_V. Thus, a phase shift of both $\pi/2$ and ϕ_V must be included. When Equation (25) is converted into phasor form and these adjustments are incorporated, the fundamental component of the output waveform can be written as:

$$\tilde{V}_{ac,fund} = \sqrt{{a_1}^2+{b_1}^2}\angle\left(\tan^{-1}\left(\frac{-b_1}{a_1}\right)+\frac{\pi}{2}+\varphi_v\right) \tag{32}$$

The root mean square, RMS, value is important in calculating THD, as it compares the RMS value of the fundamental component to the RMS value of the entire signal. The RMS value of Equation (32) is simply computed by taking the absolute value of the phasor. The controller calculates the RMS value of the entire function according to Equation (33).

$$f_{RMS} = \sqrt{\frac{1}{T_2 - T_1}\int_{T_1}^{T_2}[f(t)]^2 dt} \tag{33}$$

The function of concern here is v_{ac}, whose periodic nature within a cycle once again allows simplification of the analysis. As has been stated previously, v_{ac} repeats itself, though with

opposite polarity, twice in a single period. This function will be squared before taking the integral, so the scope of the equation can be reduced to the interval from 0-π rad instead of the entire interval, 0-2π rad. This will not change the results, but it will simplify the equation. The RMS value of the output voltage produced by the inverter is captured in Equation (34).

$$V_{ac,RMS} = \sqrt{\frac{1}{\pi}\int_0^{\pi}\left(\sum_{i=1}^{N} q_i(\theta_v)V_{C,i}\right)^2 d\theta_v} \tag{34}$$

This can be expanded,

$$V_{ac,RMS} = \sqrt{\frac{1}{\pi}\sum_{i=1}^{N}\sum_{j=1}^{N} V_{C,i}V_{C,j}\int_0^{\pi} q_i(\theta_v)q_j(\theta_v)d\theta_v} \tag{35}$$

And rewritten as:

$$V_{ac,RMS} = \sqrt{\frac{1}{\pi}{V_C}^T\delta_{i,j}V_C} \tag{36}$$

In Equation (36), V_C is an Nx1 vector that includes the values of each capacitor voltage. $\delta_{i,j}$ is an NxN matrix that captures the state of the switching functions. Notably the value in the ixj place in the δ matrix equals 1 if and only if the switching functions associated with both the i and j inputs equal one. Equations (35) and (36) cannot be expressed as functions of $\theta_{i,on}$ and $\theta_{i,off}$ because the status of each switch and its relationship to every other switch is important. As a result, the fundamental component of the output waveform can be compared to the entire output waveform, and the THD can be calculated according to Equation (37).

$$THD = \sqrt{\frac{{V_{ac,RMS}}^2 - {V_{ac,fundRMS}}^2}{{V_{ac,fundRMS}}^2}} \tag{37}$$

The control strategy seeks to reduce the THD in the output voltage waveform. To accomplish this, the controller calculates the THD initially. It then adjusts the operating times of each switch to change the shape of the waveform in attempt to reduce the harmonic content.

3.3.3 Power Factor Control

The general function of the proposed inverter is supplying power to a utility grid. In discussing power systems, the focus is often placed on complex power, S. Complex power is a combination of real and reactive power, which are represented by P and Q respectively in Equation (38)(39). The values of real and reactive power are determined based upon the magnitude of the complex power and the phase angle between the voltage and current. Although the injection of reactive power can be extremely helpful in certain higher voltage scenarios, the proposed inverter attempts to deliver strictly real power to the utility grid.

$$S = P + jQ \tag{38}$$

Certain effects introduced by specific elements in the proposed topology must be accounted for to reduce the amount of reactive power injected into the grid. As with the majority of inverters, the proposed inverter uses an inductor to filter the output current, as can be seen in Figure 3.6, and reduce undesirable distortion. An inductor acts as an energy storage device and looks like an impedance to an AC signal. When AC power flows through the inductor, this impedance changes the phase angle between the voltage and current, which changes the amount of reactive power present in the signal. The control scheme produces voltage that leads the current in order to offset the phase shift introduced by the inductor. In this way the controller minimizes the reactive power injected into the grid. The first step in this process is calculating the current flowing to the grid. This calculation can be performed according to Equation (39).

$$\tilde{I}_{ac,fund} = \frac{\tilde{V}_{ac,fund} - \tilde{V}_g}{jwL} \tag{39}$$

Equation (39) is written with respect to the fundamental components of the current and voltage. The fundamental component delivers average power to the load and is of utmost importance. Although non-fundamental components will influence the overall output, this portion of the control scheme focuses on optimizing the average power delivered to the grid and thus focuses exclusively on the fundamental component. It should be noted from Equation (32) that the inverter's output voltage, v_{ac}, is dependent upon the phase angle between the grid voltage and the output voltage of the inverter, ϕ_V. This relationship has a very strong impact on the current fed to the grid as it is calculated in Equation (39).

For the purposes of this simulation, it is assumed that the grid acts exactly as expected. It is modeled as a perfect sinusoid with an RMS voltage of $V_{g,RMS}$ = 120 V. Moreover, the phase angle of the grid voltage is set to zero for simplicity because all the phase angles are established relative to the grid voltage. These details are expressed below.

$$\widetilde{V_g} = 120\angle 0 \text{ V} \tag{40}$$

The complex power can be calculated based upon the current fed to the grid. Complex power is often defined as the product of the voltage times the conjugate of the current, which captures the relationship between the phase angles of the current and voltage. In this system, there are multiple voltages and currents, so care must be taken in identifying which values to use. To calculate the complex power delivered to the grid, one must use the grid voltage and the current injected into the grid, according to Equation (41).

$$S_g = \widetilde{V_g}\tilde{I}_{ac,fund}^{\ *} \tag{41}$$

The reactive power is easily determined from the complex power. According to Equation (38) the reactive power is simply the imaginary component of the complex power. Thus, the reactive power supplied to the grid is simply the imaginary component of Equation (41).

$$Q_g = \mathrm{Im}(S_g) \tag{42}$$

The control strategy attempts to reduce the reactive power injected into the grid. The control strategy measures the reactive power first. It then adjusts the phase angle between the inverter's output voltage and the grid voltage, ϕ_V, in order to decrease the amount of reactive power supplied to the grid. In this way the controller minimizes Q_g.

3.3.4 The Constraint

Instead of completely eliminating the reactive power and the THD present in the output waveform, the controller can only minimize the amount that is injected into the grid. The controller must account for constraints introduced by the inverter's topology when calculating operating conditions. The main constraint stems from the law of conservation of energy and Kirchhoff's Current Law. In a broad sense these laws imply that the current flowing out of the inverter must equal the current flowing into the inverter. The controller knows that the PV systems are operating near their MPP's and uses the MPP current values as an input value for calculations, as seen in Figure 3.7. The controller compares the average current produced by the PV systems to the average current injected into the grid to ensure that these values match and the laws are not violated.

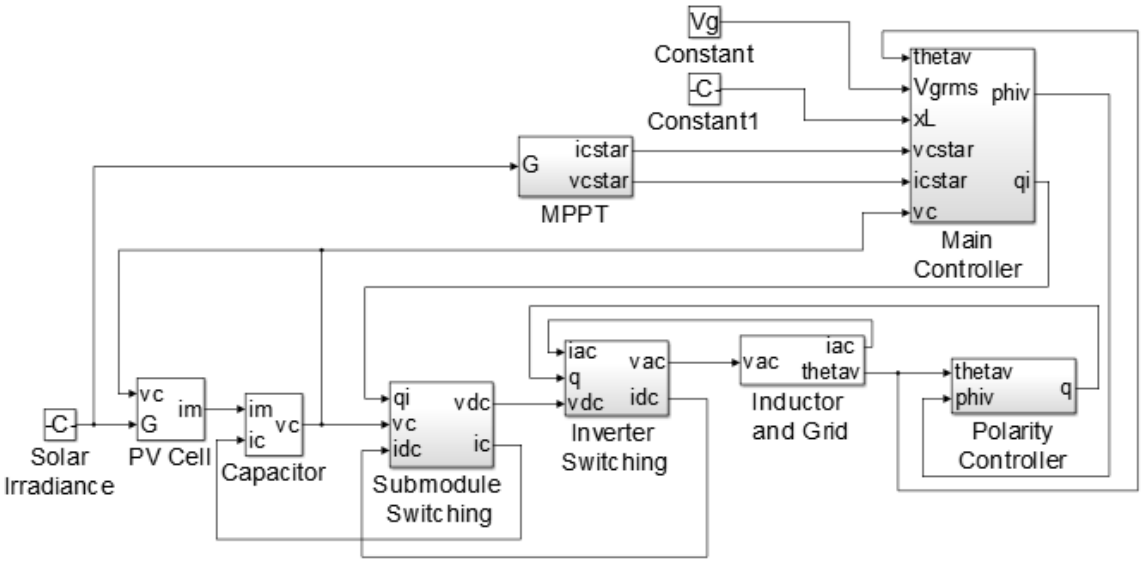

Figure 3.7: Simulink Model of entire system including PV systems, proposed inverter and grid

In accordance with KCL, when an input PV system is connected in series with the output, the current flowing through that input is equal to the current being supplied to the grid. It is necessary that the average current drawn from an input source match the average current produced by that source. This relationship establishes the constraint. It has been previously explained that the switches are connected at the same phase angle every half period. As such, one can look at the interval from 0-π rad and know that it contains the same information as the interval 0-2π rad. Of chief concern to the constraint is the average current flowing through an input, $\bar{\imath}_i$, which is expressed as a function of the output current and the switching function associated with that input.

$$\overline{\iota_i} = \frac{1}{\pi}\int_0^{\pi} q_i(\theta_v) I_{ac,fund}(\theta_v) d\theta_v \tag{43}$$

The term $I_{ac,fund}(\theta_V)$ is equivalent to the phasor value presented in Equation (39), just rewritten in a different form. The variables introduced in its definition below, $I_{ac,fundRMS}$ and ϕ_I, are

simply the magnitude and phase angle associated with the fundamental component of the output current. These can be easily determined from the phasor form.

$$I_{ac,fund}(\theta_v) = \sqrt{2} I_{ac,fundRMS} \sin(\theta_v - \varphi_V + \varphi_I) \tag{44}$$

When the *i*-th switch is closed, current flows through the *i*-th input. This is the only time that the output current flows through the input system and contributes to the average current flowing through the input over the course of the period. As a result, Equation (43) can be rewritten with respect to $\theta_{i,on}$ and $\theta_{i,off}$ to focus exclusively on the intervals when the switch is closed.

$$\overline{i_i} = \frac{\sqrt{2}}{\pi} I_{ac,fundRMS} \begin{cases} \int_{\theta_{i,on}}^{\theta_{i,off}} \sin(\theta_v - \varphi_V + \varphi_I)\, d\theta_v, & \theta_{i,on} < \theta_{i,off} \\ \int_{0}^{\theta_{i,off}} sin(\theta_v - \varphi_V + \varphi_I)\, d\theta_v + \int_{\theta_{i,on}}^{\pi} sin(\theta_v - \varphi_V + \varphi_I)\, d\theta_v, & \theta_{i,off} < \theta_{i,on} \end{cases} \tag{45}$$

Taking the integral yields:

$$\overline{i_i} = \frac{\sqrt{2}}{\pi} I_{ac,fundRMS} \begin{cases} \cos(\theta_{i,on} - \varphi_V + \varphi_I) - \cos(\theta_{i,on} - \varphi_V + \varphi_I) & \theta_{i,on} < \theta_{i,off} \\ 2\cos(-\varphi_V + \varphi_I)\cos(\theta_{i,on} - \varphi_V + \varphi_I) - \cos(\theta_{i,on} - \varphi_V + \varphi_I) & \theta_{i,off} < \theta_{i,on} \end{cases} \tag{46}$$

This average current is then calculated according to Equation (46). Simultaneously, the MPPT technique, described in Section Maximum Power Point Tracking, calculates the current that the PV systems produce. The controller compares these two currents. The difference between these two currents must equal zero. This equation represents the constraints that must be met when the controller minimizes THD and reactive power.

3.4 Simulink Implementation

The Main Controller block shown in Figure 3.7 executes the control strategy for the proposed inverter. Figure 3.8 shows a more detailed view of the controller block as it exists in the Simulink model. The inputs are fed to the Interpreted MATLAB Function block that runs a script to calculate the optimal switching times for the switches. The script essentially analyzes the

inverter's performance and modifies the appropriate variables to improve the performance. The block executes the script once every cycle to periodically update the control parameters and ensure optimal performance of the inverter.

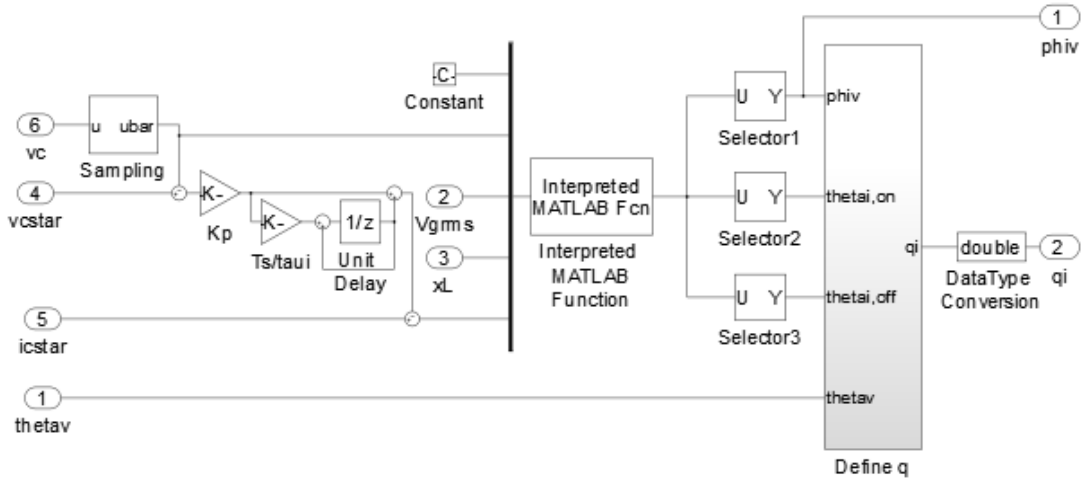

Figure 3.8: Simulink subsystem that constitues the main controller of the proposed inverter

The Matlab script executed by the Interpreted MATLAB Function block uses the Matlab function *fmincon*. This command attempts to find solutions for functions that contain several interdependent variables. Due to the presence of a constraint, absolute solutions for these variables do not exist. The command *fmincon* performs a type of minimization so as to produce values for the variables that satisfy the function as closely as possible under the defined constraint. The script uses Equations (30) - (32), (36), and (39) to quantify the important characteristics of the output. The script compares the results of Equation (46) to the MPP current. This comparison constitutes the constraint in *fmincon* that cannot be violated because the average current flowing out of the inverter must equal the current being delivered to the inverter. Equation (37) and (42) are executed to calculate the distortion in the output, THD, and the reactive

power delivered to the grid, Q_g. The function *fmincon* attempts to minimize these two variables by adjusting the values of ϕ_V, $\theta i_{,on}$ and $\theta_{i,off}$.

3.5 Comparable VSI Inverter

The performance of the proposed inverter is compared to that of a string inverter due to the similarities between the two topologies. Each topology uses the conglomerated output of multiple PV panels. Both are capable of producing the same level of power. Both inverters produce voltage at the utility grid level without using any voltage gain techniques. The string inverter uses the VSI control technique to be comparable to the low frequency switching used by the proposed inverter. Despite these strong parallels, the model of the string inverter developed in Simulink is noticeably different than the model of the proposed inverter. The Simulink model is shown in Figure 3.9.

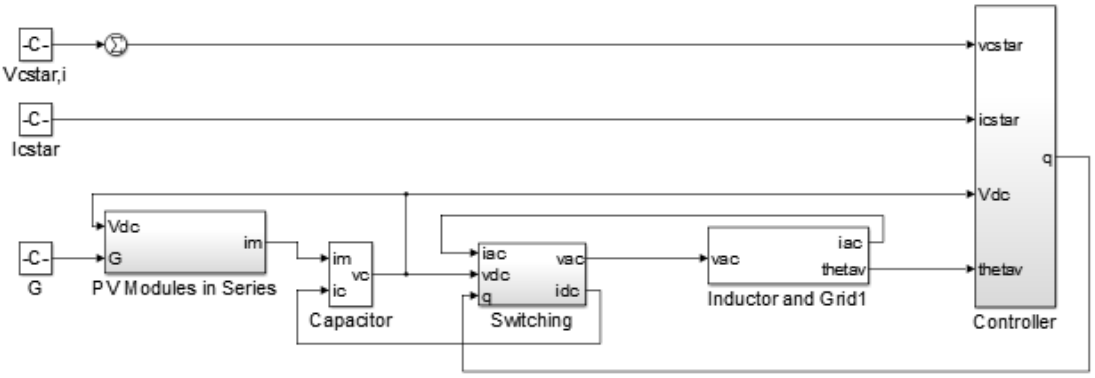

Figure 3.9: VSI developed in Simulink

One major difference between the two Simulink models is how the PV modules operate relative to one another. In the proposed inverter, each PV module operates independently. In the string inverter, the PV modules are all connected in series and the performance of one module affects the performance of all the others. The same general approach described previously is

taken to simulate the behavior of the PV modules for the VSI, but a different mathematical relationship exists to capture the series connection between modules.

Equation (16) still describes the performance of an individual PV module. For the proposed inverter, this equation is solved individually for each PV module because the current, voltage and solar irradiance associated with one PV module are independent of any other module. When Equation (16(16) is applied to each PV module in the VSI inverter – portrayed in Equation (47) – multiple equations are introduced that share the unknown variable I_M. This establishes a system of non-linear equations that must be solved collectively.

$$f_i = \frac{G}{G_{ref}} \times I_{sc} - \frac{V_{C,i}}{R_P} - I_M \times \left(1 + \frac{R_S}{R_P}\right) - I_{sat}\left(e^{\left(\frac{q(V_{C,i}+R_S \times I_M)}{N_s nkT}\right)} - 1\right) = 0, \quad i = 1,2,\dots,n \quad (47)$$

There are *n*+1 unknown variables introduced in Equation (47) but only *n* functions. The unknown variables include the output voltage of each PV module, $V_{C,i}$, and the common current flowing through each module, I_M. The voltage output of the entire PV system, V_{dc}, equals the sum of the voltages produced by each PV module because the modules are connected in series. This relationship is depicted in Equation (48) and is important because it introduces a new equation without introducing any new unknown variable.

$$f_{n+1} = V_{dc} - \sum_{i=1}^{n} V_{C,i} = 0 \quad (48)$$

One must apply the Newton-Raphson method to solve this system of equations. To do this, all the unknown variables are combined into a single vector variable, *x*, according to Equation (49). Similarly, each equation is included in a vector that comprises a single vector-valued function, f(*x*). Unlike the Newton method, a simple derivative of this function cannot be calculated due to the multivariable nature of the *x*. the Jacobian matrix, J(*x*), must be used to include all the partial derivatives of the function.

$$x = [V_{C,1}, V_{C,2}, \dots, V_{C,n}, I_M]^T \tag{49}$$

$$f(x) = [f_1, f_2, \dots, f_n, f_{n+1}]^T \tag{50}$$

$$J(x) = \frac{\partial}{\partial x} f(x) = \begin{bmatrix} \frac{\partial}{\partial V_{C,1}} f_1 & \cdots & \frac{\partial}{\partial I_M} f_1 \\ \vdots & \ddots & \vdots \\ \frac{\partial}{\partial V_{C,1}} f_{n+1} & \cdots & \frac{\partial}{\partial I_M} f_{n+1} \end{bmatrix} \tag{51}$$

The Newton-Raphson method uses the Jacobian matrix to solve for the unknown variable *x*. This deviation from the Newton method is captured in the following equation.

$$x^{k+1} = x^k - \alpha J^{-1}(x^k) f(x^k) \tag{52}$$

A simple script is written in Matlab to execute five iterations of the Newton-Raphson method presented in Equation (52). This script is incorporated into the Simulink model of the PV systems for the VSI inverter using the Matlab function block. This block executes the code as necessary. This implementation is shown in Figure 3.10.

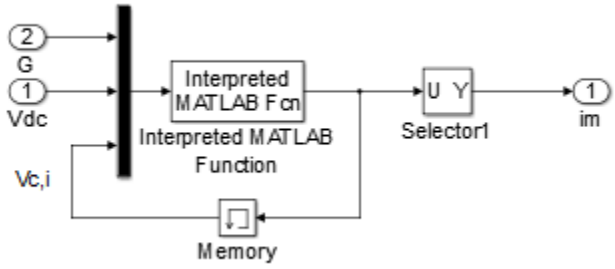

Figure 3.10: Model of PV system for VSI inverter

The approach taken to implement these equations in the Simulink model for the VSI inverter is slightly different than that taken for the proposed inverter. The VSI uses a simple script, whereas the proposed inverter uses the basic Simulink blocks to implement the appropriate

equations and execute the necessary number of Newton steps. The performance of the Simulink model does not change regardless of the way that the equations are implemented. The alternate approach is used for the VSI inverter merely out of convenience. Both approaches use the same number of iterations, use the same convergence rate, α, and produce models of PV systems that accurately simulate the performance of real PV modules.

As was the case with the proposed inverter, a simple approach can be used to perform MPPT in lieu of more complex techniques. The MPPT seeks to find the current and voltage levels that maximize the output power for the entire collection of PV modules. The script designed to perform MPPT uses the *fsolve* and Equation (47) to identify the I-V curves for each PV module based on the level of solar irradiance. Each PV module must have the same amount of current flowing through it, so the script calculates the total power produced by the group of PV modules by summing the corresponding voltages of each PV module and multiplying them with the current, as shown in Equation (53). This step of calculating power is repeated over the range of all possible currents. The level of current and the corresponding voltages that produce the maximum amount of power are identified as the MPP. These values are fed into the VSI controller.

$$P = \sum_{i=1}^{n} \left(V_{C,i}\right) \times I_M, \qquad I_M \in [0, I_{SC}] \tag{53}$$

There are only two variables over which the VSI inverter has control: the phase delay angle and the angle of displacement. The controller is trying to solve an optimization problem. The VSI controller must calculate the phase delay angle, ϕ_V, and the displacement angle, δ, that minimize the reactive power delivered to the grid and push the inverter to operate near the MPP. Figure 3.11 shows that the Matlab function that solves the optimization problem provides values for these two variables.

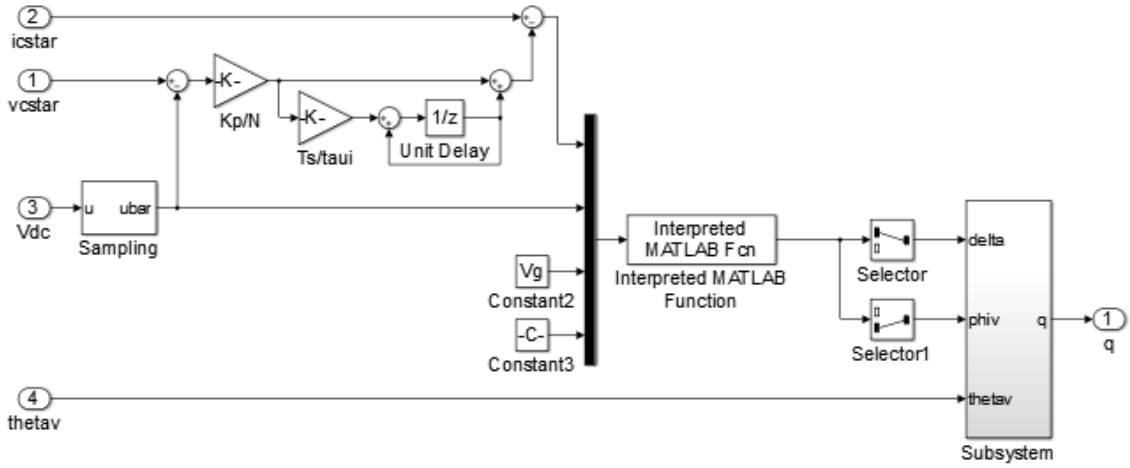

Figure 3.11: Simulink subsystem for VSI controller

A voltage source inverter produces a well-defined output waveform that is easily described in generic form by the Fourier series [12]. The VSI controller focuses on the fundamental component of the output because it is the only component capable of transferring average power to the grid. The fundamental component of the general Fourier series describing the output of the VSI is adapted to the current implementation to be expressed in terms of the relevant variables discussed in the previous paragraph. The equation is presented in polar form in Equation (54).

$$\tilde{V}_{ac,fund} = \frac{2\sqrt{2}}{\pi}\cos\left(\frac{\delta}{2}\right)e^{j\varphi} \tag{54}$$

Just like the calculations for the proposed inverter, the fundamental voltage can be used to calculate the fundamental current. The phasor form is being used for calculations, but the current is also written to show the magnitude and phase angle of the fundamental current.

$$\tilde{I}_{ac,fund} = \frac{\tilde{V}_{ac,fund} - \tilde{V}_g}{jwL} = \left|I_{ac,fund}\right|\angle\varphi_i \tag{55}$$

The phasor, $\tilde{I}_{ac,fund}$, must be converted into an instantaneous value, $i_{ac,fund}$, to quantify the amount of current produced by the inverter over the course of one cycle.

$$i_{ac,fund} = \sqrt{2}\left|I_{ac,fund}\right| \sin\left(\theta_g + \varphi_i\right) \tag{56}$$

The fundamental current is used to calculate the average current delivered to the grid.

$$\bar{\imath}_{dc} = \frac{1}{2\pi}\int_0^{2\pi} i_{ac,fund}\, di \tag{57}$$

The instantaneous current is rewritten in terms of the switching times, θ_{on} and θ_{off}, of each switch. $\theta_{on,1}$ corresponds to the phase angle at which the switch labelled q_{11} in Figure 2.3 turns on or closes. $\theta_{on,2}$ corresponds to the phase angle at which the switch labelled q_{22} closes.

$$\bar{\imath}_{dc} = \frac{\sqrt{2}\left|I_{ac,fund}\right|}{2\pi}\left[\int_{\theta_{on,1}}^{\theta_{off,1}} \sin\left(\theta_g + \varphi_i\right) d\theta_g + \int_{\theta_{on,2}}^{\theta_{off,2}} \sin\left(\theta_g + \varphi_i\right) d\theta_g\right] \tag{58}$$

The switching times for each switch, θ_{on} and θ_{off}, can be expressed in terms of the displacement angle, δ, and the phase delay angle between the grid voltage and the inverter voltage, ϕ_V. The VSI inverter closes each switch for half of the cycle, so it follows that the switches open π rad after they close.

$$\theta_{on,1} = -\varphi_v - \frac{\delta}{2} \tag{59}$$

$$\theta_{off,1} = -\varphi_v + \frac{\delta}{2} \tag{60}$$

$$\theta_{on,2} = -\varphi_v - \frac{\delta}{2} + \pi \tag{61}$$

$$\theta_{off,2} = -\varphi_v + \frac{\delta}{2} + \pi \tag{62}$$

Solving for the integral in Equation (58) and plugging in Equations (59) – (63), the average current produced by the inverter can be written as a function of the two variables over which the VSI controller has control: ϕ_V and δ.

$$\bar{\imath}_{dc} = \frac{2\sqrt{2}}{\pi} I_{ac,fund} \cos(\varphi_i - \varphi_v) \cos\left(\frac{\delta}{2}\right) \tag{63}$$

The VSI controller uses the Matlab function *fsolve*, to calculate the phase delay angle and the displacement angle that simultaneously minimize reactive power injected into the grid and push the average power of the inverter to operate closer to the MPP.

4 Results

It first will be demonstrated that the PV model and MPPT perform as expected to show that the model simulates the performance of a real PV system. The inverter's performance is then compared to a comparable VSI inverter to demonstrate the inverter's capabilities.

The proposed system is tested to ensure that it performs as desired. Finally the performance of the proposed inverter is evaluated based upon its ability to meet standards and through a comparison with comparable inverters.

4.1 Simulink Model of PV System and MPPT

The Simulink model that is developed in this paper is used to simulate the output of a real photovoltaic panel (Grape Solar model: GS-P-280-Fab1). Values for various variables used in the mathematical model of Equation (14) are extracted from the PV manufacturer's data sheet, which can be found in APPENDIX A. The model uses a value of 1.17 for the ideality factor in the Shockley diode equation to adjust the output of the single-diode model to more accurately match the performance of an actual PV panel.

The Simulink model of a PV panel successfully simulates the output of a real PV panel under STC. Table 4.2 focuses on several points from a panel's I-V curve that are typically used in the industry to describe the performance of the panel. The table shows the value for these points that are listed on the data sheet furnished by the manufacturer and the value of these points on the I-V curve produced by the Simulink model of the PV panel under STC. In this way, the table compares the performance of the Simulink model to an actual PV panel. The values produced by the PV model are with are within 2% of the values provided on the data sheet. The data sheet indicates that the performance of actual panels may vary from the listed values by as much as 3%. Thus, the Simulink model performs within the tolerance limits specified on the data sheet.

Table 4.1: Comparison of the Simulink model and the manufacturer's data sheet at STC

Source:	P_{MPP} (w)	V_{MPP} (V)	I_{MPP} (A)	V_{OC} (V)	I_{SC} (A)
Data Sheet	280.0	35.8	7.8	44.6	8.4
Simulink Model	275.8	35.3	7.8	45.4	8.4
% Difference	1.5	1.5	0.0	1.7	0.1

For the purposes of this paper, the Simulink model of the PV panel must function in a similar, though not necessarily exact, fashion as a real panel in order to demonstrate the inverter's ability to respond to realistic situations. The data in Table 4.1 indicates the model does simulate the performance of a real PV panel under STC. The performance of the actual PV panel when exposed to conditions other than STC is not readily provided by the manufacturer, so the performance of the Simulink model under different conditions cannot be assessed in a mathematically precise manner. Figure 4.1 does show that under different conditions, the Simulink model does produces appropriately shaped I-V curves and in general produces less power when exposed to lower levels of solar irradiance. This performance is consistent with that of an actual PV panel, so it can be said that the Simulink model accurately simulates the performance of a real PV model to the extent required for this application.

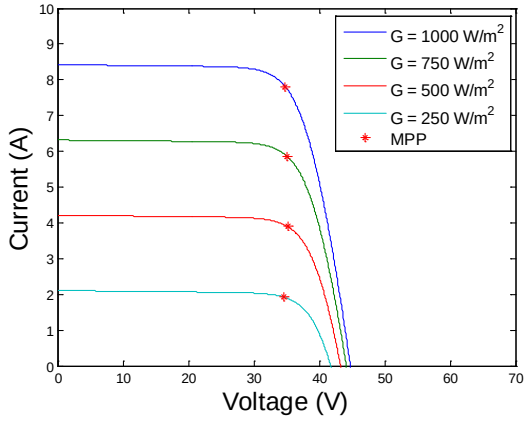

Figure 4.1: I-V curves from the Simulink model of a PV panel exposed to different irradiance levels

As described in Section Adjusting the Model to the Whole System, the Simulink model of the single PV panel is adjusted to model a PV module, still successfully simulating the realistic performance of a PV system but not necessarily corresponding to the performance of a specific PV panel currently on the market. The values for all of the system parameters after these adjustments have been made are presented in the table below.

Table 4.2: System parameters for the Simulink model

Variable Name	Symbol	Value	Units
Solar Irradiance at STC	Gref	1000	W/m^2
Short Circuit Current	Isc	8.43	A
Open Circuit Voltage	Voc	56.725	V
Cells in series	Ns	90	
Operating Temperature	T	298	K
Shunt Resistance	R_P	0.6625	Ω
Series Resistance	R_S	662.5	Ω
Reverse Saturation Current	I_{sat}	6.60E-09	A
Diode Ideality Factor	n	1.17	
Independent PV Modules	N	4	
Output Filter Inductance	L	17	mH
PV Capacitance	C	9.2	mF
Sampling Time	Ts	16.67	ms
Initial Voltage	$V_{C,0}$	43.75	V
Controller Input Adjustment Factor	τ	0.33	s
Controller Input Signal Gain	K_P	0.2	
Newton Method Convergent Rate #1	alpha	1	
Newton Method Convergent Rate #2	alpha2	0.8	
Grid Voltage, rms	Vg	120	V
Grid Angular Frequency	omega	377	rad/sec
Elementary Charge	q	1.60E-19	C
Boltzmann's Constant	k	1.38E-23	J/K

The MPPT block in Simulink accurately predicts the voltage and current associated with the maximum power point. The current and voltage levels of the MPP as produced by the MPPT block are compared to the voltage and current levels that create maximum power based upon the I-V curves produced by the PV model. The Simulink block performing MPPT independently

calculates the exact same voltage and current levels of the MPP that are deduced from the I-V curves in Figure 4.1. This is a result of the fact that the Simulink PV models and the MPPT blocks use the same equations as a basis for their calculations. Thus, the MPPT block performs as expected.

4.2 General Output of the Inverter

The inverter converts the input DC voltages supplied by the PV modules into a multilevel output waveform. The output voltage is a nine level waveform because the inverter has four DC voltage sources, where each source is an independently operating PV system. The output oscillates between roughly 180 V and -180 V at 60 Hz by design to match the grid voltage. Figure 4.1a shows the output voltage produced by the inverter and its calculated fundamental component. The output waveform bears close resemblance to a sine wave, which indicates the controller is operating correctly and producing the desired output waveform.

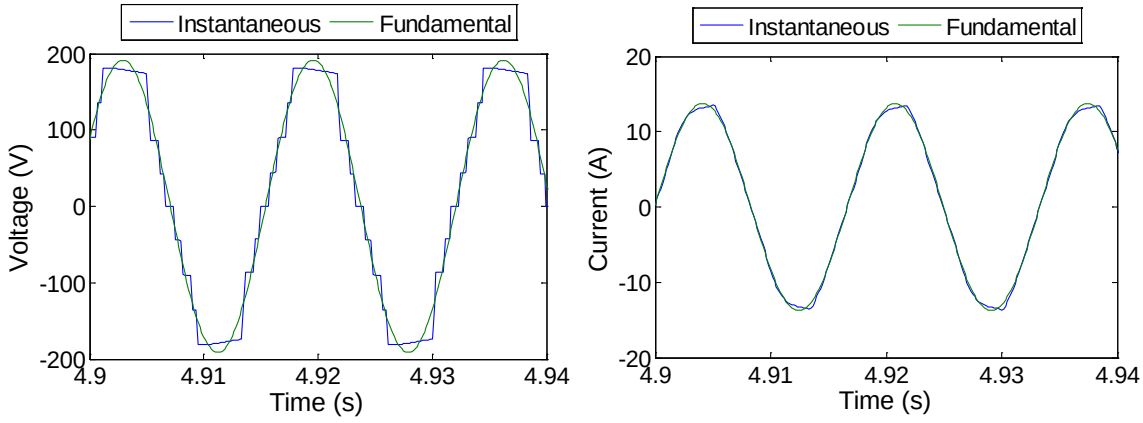

(a) (b)

Figure 4.2: The raw outputs and their 60 Hz components

Table 4.3 shows the input conditions that produce the output above. The solar irradiance is the input variable that affects the performance of the PV panel. The table shows that each PV

module is exposed to a different level of solar irradiance. The MPPT block in Simulink calculates currents and voltages associated with the maximum power point per individual PV module based upon the solar irradiance input. Those currents and voltages are documented in the table below under the heading "Expected MPP." The maximum power that the PV module can theoretically produce is calculated using those current and voltage levels and is documented in the P_{MPP} column. In the same fashion, the actual voltage and current produced by each PV module are recorded in the table under the "Actual Output" heading. These values are multiplied together to calculate the power produced by each module.

Table 4.3: Performance of Simulink PV modules

PV Module	Solar Irradiance (W/m^2)	Expected MPP			Actual Output		
		P_{MPP} (W)	V_{MPP} (V)	I_{MPP} (A)	P_{max} (W)	$V_{C,RMS}$ (V)	$I_{M,RMS}$ (A)
1	1000	345	44.10	7.82	344	44.11	7.80
2	900	312	44.28	7.04	311	44.28	7.02
3	800	278	44.44	6.25	277	44.44	6.24
4	700	244	44.55	5.47	243	44.55	5.46

The table indicates that the controller allows the individual PV modules to operate near their expected MPP. Furthermore, the table reveals that the PV modules operate as expected. Figure 4.1 indicates that the voltage of the MPP of each module should be roughly the same while the currents produced by each module should be noticeably different. The table supports that relationship.

Figure 4.3 shows the instantaneous current and voltage drawn from the input PV systems and capacitors. The legend identifies Input 1 through Input 4, which correspond to the individual PV systems serving as DC voltage source inputs for the inverter. There exists a small ripple in the output from the PV systems. This ripple occurs because the inputs are periodically connected in

series with the output. Connecting the input causes current to flow out of the capacitor. This act discharges the capacitor and lowers the voltage potential across its terminals. Bypassing the input allows the capacitor voltage to recharge. To compare the voltage and current produced by the PV systems to the DC MPP operating points identified by the MPPT block, the RMS values of the ripples are calculated. The controller and inverter are performing well because they draw the maximum power possible from the inputs.

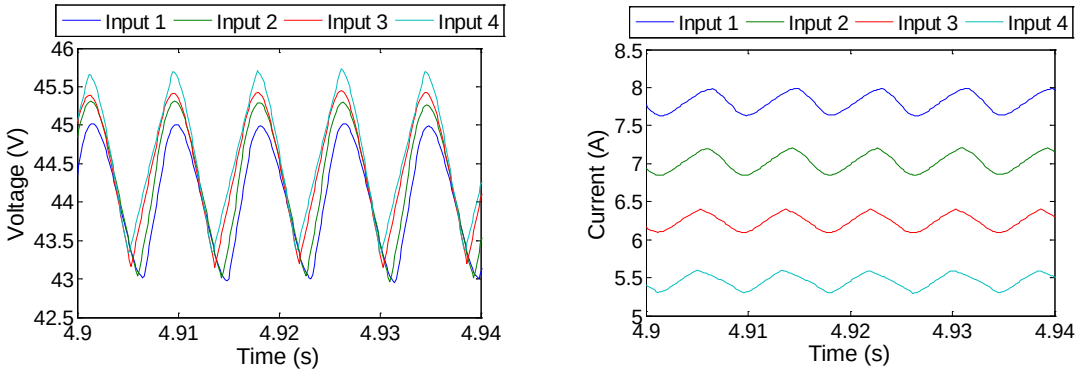

(a) (b)

Figure 4.3: The voltages and currents produced by each PV module

Each PV module produces voltage at roughly the same level, but the modules generate noticeably different amounts of current. The voltages stay within 2 % of one another at all times. There is a general trend that is observed in Table 4.3 but is more easily noticed in Figure 4.3. When the PV module is exposed to lower levels of solar irradiance, the voltage level tends to increase slightly while the current and power levels decrease substantially. The controller needs to combine the voltages in a specific manner to produce the desired 9-level output waveform but is constrained by the fact that the average current produced by the inverter must equal the average current generated by the PV modules. The current produced by the modules heavily influences the timing when each module is connected because the relationship between current and solar irradiance has the largest impact on the constraint.

Figure 4.4 shows the time that each module is connected every half cycle. The horizontal axis indicates the time elapsed during the simulation. The vertical axis represents the phase angle of the grid voltage as it occurs once every cycle of the simulation. The lower four lines of the figure represent $\theta_{ON,i}$ for each PV module. It is at this point in every cycle that the module is connected, which produces a step up in the output waveform of the entire inverter. The upper four lines in the figure show when each PV module is disconnected, $\theta_{OFF,i}$, and represent a step down in the output waveform. Both $\theta_{ON,i}$ and $\theta_{OFF,i}$ fluctuate slightly from one cycle to the next.

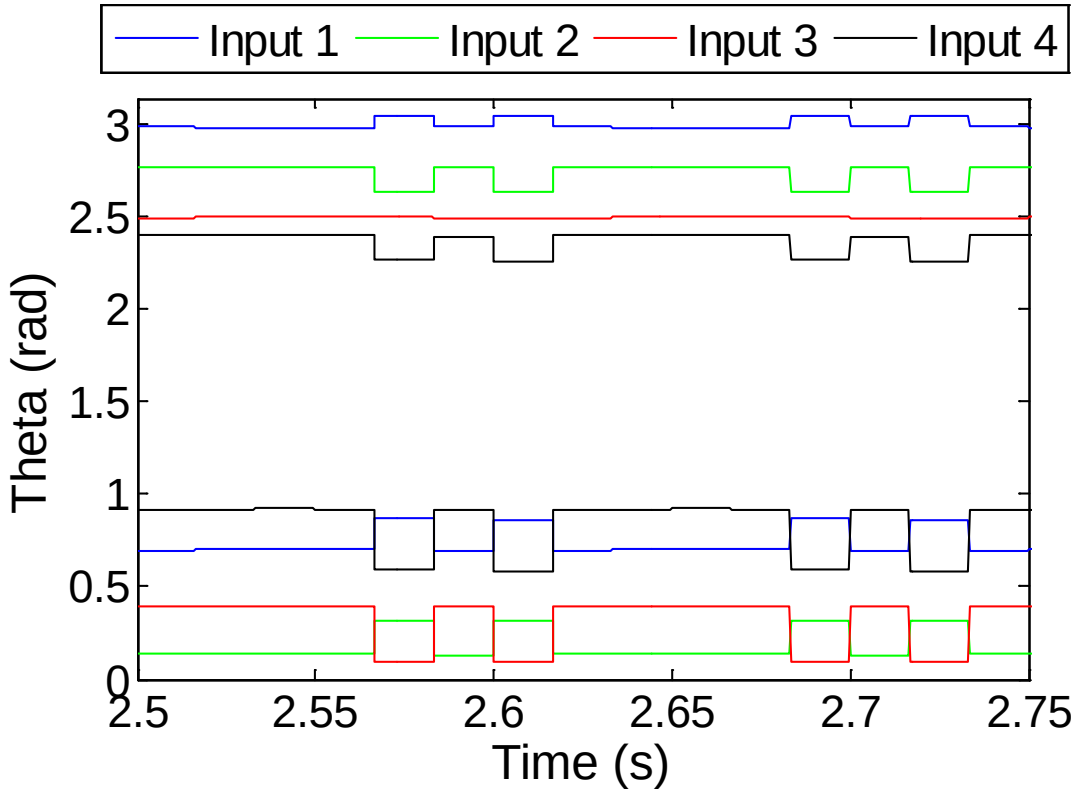

Figure 4.4: Graphical representation of input switching times

The figure above indicates the controller successfully assigns distinct times when each input is connected. When each PV module produces current at a different level, the controller assigns distinct times when each module will be connected and disconnected ($\theta_{ON,i}$ and $\theta_{OFF,i}$). In

the figure, there is a slight fluctuation in the switching times of each module. This fluctuation itself is a pattern that repeats itself roughly every 0.1 sec. The cause of the fluctuation is unknown, but is a good topic warranting further investigation.

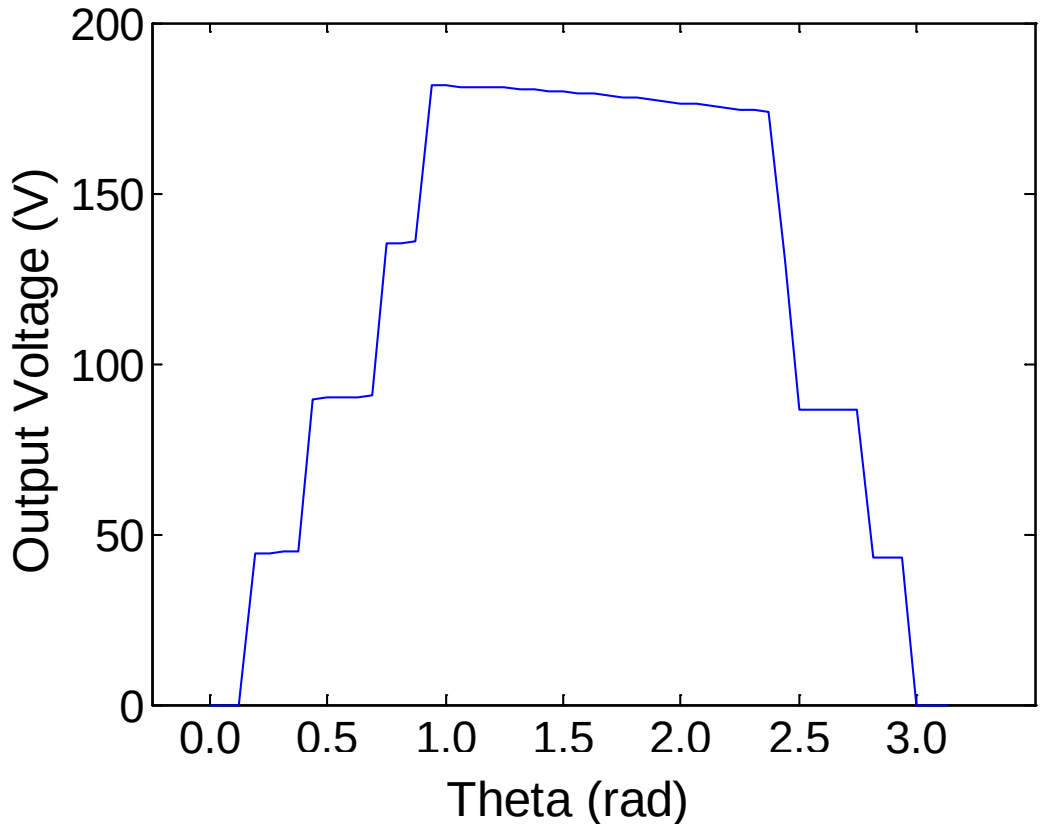

Figure 4.5: Positive half-wave produced by inverter twice per cycle

The controller coordinates connecting each input in order to produce an output voltage with a roughly sinusoidal waveform. Figure 4.5 shows the stepped waveform produced as a function of the phase angle. The x-axis in Figure 4.5 corresponds to the y-axis in Figure 4.4. These values are listed in the table below.

Table 4.4: Average switching time of input every half cycle

Input	θ_{ON} (rad)	θ_{OFF} (rad)
1	0.75	3.00
2	0.18	2.73
3	0.32	2.50
4	0.83	2.37

While coordinating switching times for each input, the controller aims to reduce the harmonic content in the output current and minimize the reactive power injected into the grid. The THD of the output current is 2.8 % with respect to the rated current fundamental. The harmonic content in the output is below the maximum allowable amount described in the IEEE standard, indicating the controller adequately minimized distortion in the output waveform. The controller also effectively minimizes reactive power injected to the grid when compared to the total complex power produced by the inverter. Although the MPPT predicts the PV panels can produce 1178 W, the panels actually produce only 1176 W. The inverter delivers 1164 W and 2.8 Var to the grid. The inverter does well in delivering 98.8 % of the theoretical maximum power that the panels can produce. The controller accomplishes its goal of minimizing the reactive power delivered to the grid by keeping the reactive component down to 0.204% of the real power injected into the grid.

4.3 Exploring Different Scenarios

To examine the capabilities of the inverter, the input PV modules are exposed to varying levels of solar irradiance in different scenarios. The performance of the inverter is recorded for each scenario and the results are compared to the performance of a comparable VSI inverter.

The six scenarios used to test the versatility of the inverter are presented in Table 4.5. The first scenarios simulate balanced conditions where the solar irradiance is evenly distributed between each PV module. These conditions serve to show the general relationship between the

solar irradiance input and the power output. The other scenarios introduce unbalanced conditions to test the performance of the inverter in real-world situations where the output of each PV panel would be affected by external factors such as shading. In the simulations, the difference between levels of solar irradiance from one panel to the next are relatively high and represent more extreme conditions than would normally occur in typical installations.

Table 4.5: The solar irradiance (W/m^2) that each input is exposed to in the different scenarios

	Solar Irradiance (W/m^2)					
Scenario / Input	**1**	**2**	**3**	**4**	**5**	**6**
1	1000	250	625	475	700	1000
2	1000	250	625	575	800	1000
3	1000	250	625	675	900	500
4	1000	250	625	775	1000	1000
Total:	4000	1000	2500	2500	3400	3500

Each scenario elicits a similar response from the inverter as the one described in the previous section. In every case, the output voltage produced by the inverter is a nine-level waveform, and the RMS value of the fundamental component of each output voltage waveform is at least 120 V. Additionally, the PV modules operate within 0.25% of their expected MPP. As such, the controller satisfactorily performs its chief objective of producing a roughly sinusoidal grid-level output voltage while simultaneously extracting the maximum amount of power from each PV module.

The information presented in Table 4.6 describes the output of the inverter under the different scenarios to help assess the performance of the inverter with respect to its secondary objectives: minimizing the harmonic content and reactive power in the output delivered to the grid. Each column, except that farthest to the left, corresponds to one of the scenarios described in the previous table. The first row, $P_{MPP,}$ displays the theoretical maximum power that the PV

panels could produce according to the MPPT Simulink block. The row below shows the average power delivered to the grid by the inverter, and the row below that includes the reactive power injected to the grid. The second row from the bottom presents the displacement power factor, which is an indicator of the phase displacement between voltage and current. The displacement power factor is calculated using the real and apparent power of the fundamental component of the current injected into the grid. The bottom row of the table reveals the harmonic content present in the current injected into the grid as quantified in terms of the Total Harmonic Distortion.

Table 4.6: Output data from proposed inverter during simulations

Scenario	**1**	**2**	**3**	**4**	**5**	**6**
P_{MPP} (W)	1379	337	871	869	1178	1208
P_{ave} (W)	1363	336	864	863	1166	1196
Q_{fund} (Var)	-14.3	4.4	17.9	5.7	2.4	-14.0
PF_{DISP}	0.999	0.999	0.999	1.000	1.000	0.999
THD_i (%)	7.3	5.7	6.5	4.0	2.8	9.9

There is less than 10% THD in the output current produced in each scenario. The low-frequency switching produces the distortion in the output current waveform. The inductor used as a filter helps to smooth the current injected into the grid and minimize the harmonic content. The harmonics exist at low frequencies making them inherently difficult to filter. For low voltage and power situations, this level of harmonic content is permissible, although less distortion is preferable.

The filter creates a phase shift between the current and voltage, which introduces reactive power. Table 4.6 shows that the amount of reactive power delivered to the grid is less than 2.1% of the average real power delivered to the grid. While this is not zero, it is less reactive power than what is introduced by the inductive filter. These numbers prove that the controller effectively minimizes the reactive power that is delivered to the grid by adjusting the phase angle

of the output voltage of the inverter. The amount of reactive power produced by the proposed inverter can be compared to that produced by a comparable VSI inverter to assess the performance of the proposed inverter.

A comparable VSI inverter is tested under the same scenarios as the proposed inverter, and the results are documented in Table 4.7. Just like the table above, the first row in Table 4.7 shows the maximum power the PV cells are capable of producing under the given conditions. The table also shows the real and reactive power supplied to the grid by the inverter as well as the amount of harmonic content in the output current.

Table 4.7: Results of the tests performed on the comparable VSI inverter

Scenario	**1**	**2**	**3**	**4**	**5**	**6**
P_{MPP} (W)	1379	337	871	736	1069	806
P_{ave} (W)	1362	336	864	729	1055	798
Q_{fund} (Var)	-4.6	10.1	-33.6	40.1	6.5	-39.1
PF_{DISP}	1.000	0.999	0.999	0.998	1.000	.999
THD_i (%)	8.4	14.9	13.0	18.3	14.5	20.5

Under balanced conditions, the VSI inverter performs very similarly to the proposed inverter. Each inverter has the same theoretical MPP and delivers the same amount of average power to the grid. In these scenarios there is more harmonic content in the output current produced by the VSI inverter than the proposed inverter. This is consistent with the literature surrounding the methods that each technique uses to invert the DC input to an AC output: the waveform with more steps is more sinusoidal and has less harmonic content. Both inverters inject little reactive power to the grid relative to the real power they supply. In every scenario except for Scenario 1, the proposed inverter injects less reactive power into the grid than the VSI inverter.

The data indicates that the proposed inverter is better suited to deliver more power under unbalanced conditions than the VSI inverter. In Scenarios 4 through 6, the distribution of the solar irradiance to an individual panel varies from one PV module o the next. The average power

delivered by both inverters is within 98.5% of the theoretical maximum that the PV modules can produce. This proves the controllers of each model effectively push the PV modules to operate near their MPP and thus work as expected. However in the unbalanced scenario, the theoretical MPP of the VSI inverter is anywhere from 10-30% lower than the theoretical MPP of the proposed inverter. An innate limitation introduced by the topology of the VSI inverter prevents the PV modules from producing as much power when there is an imbalance in the distribution of solar irradiance. This is expected because of the negative effect of shading on string inverters that is well documented in literature. Shading has a much smaller effect on the power produced by the proposed inverter because the PV modules are able to operate independently of one another.

Unbalanced conditions hinder the ability of the VSI inverter to minimize harmonic distortion, but do not appear to have the same effect on the proposed inverter. Scenarios 3 and 4 expose the PV systems to the same level of solar irradiance, collectively, but Scenario 3 exposes each PV system to the same level of solar irradiance while Scenario 4 exposes each system to a different level. The level of THD and reactive power delivered to the grid by the VSI inverter increase by 41% and 19% respectively in unbalanced conditions relative to balanced conditions. The imbalance causes the inverter to forfeit some of its control over the quality of the output in order to continue to maximize the quantity of the output power. The inverter still performs respectably, but the tradeoff is apparent. For the proposed inverter, the measured THD and reactive power stay low and actually decrease in the unbalanced scenario. By allowing each PV module to operate independently and combining their outputs at the most opportune times, the proposed inverter can continue to maximize power production without sacrificing quality when conditions are unbalanced.

Certain scenarios that represent extreme and unrealistic conditions actually prevented the inverter from operating near the theoretical MPP. These scenarios introduced large

differences in the amount of solar irradiance distributed to each PV module, on the order of 750 W or 75% of STC conditions. In these scenarios the Matlab function calculating the switching times and the phase angle would stop prematurely and could not push the inverter to operate in a stable state. Additional testing showed the MPPT failed to converge in these highly unbalanced conditions, and as a result the MPPT fed incorrect target values to the controller. The controller was functioning as expected and could not complete the calculations because of faulty input data resulting from incorrect assumptions made about the inverter. This can be prevented in future testing by using a dynamic and more robust MPPT technique.

The proposed inverter is designed to excel under unbalanced conditions. The control strategy that allows for the inverter's stellar performance under unbalanced conditions also helps the controller under semi-balanced and balanced conditions. A closer examination of the inverters performance during one scenario reveals the key behind the inverter's performance. In every scenario the controller assigns a distinct time to each input that establishes when the input is connected and bypassed. In the initial scenario mentioned above, each input has the same θ_{ON} and θ_{OFF} every cycle. In another scenario, those times change from one cycle to the next for a given input, as seen in the figure below.

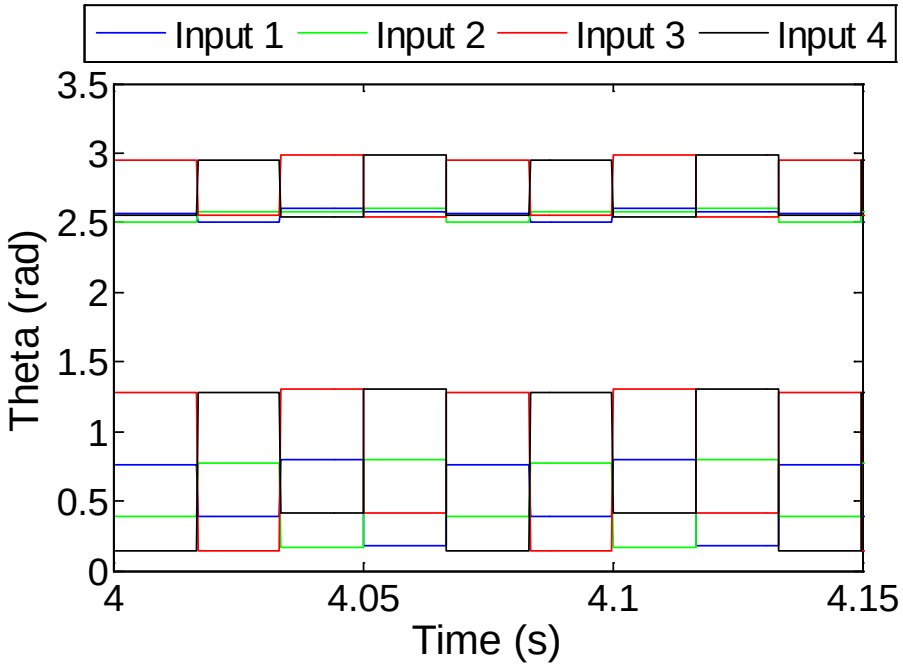

Figure 4.6: The switching times of each input PV modules

The figure above shows the switching times, $\theta_{ON,i}$ and $\theta_{OFF,i}$, of the input PV modules when a pair of modules are exposed to the same level of solar irradiance. In this scenario, Input 3 and 4 are both exposed to G = 450 W/m^2. During one cycle, the turn on and turn off times for Input 3 are $\theta_{ON,3}$ = 1.42 rad and $\theta_{OFF,3}$ = 2.93 rad. The turn on and turn off times for Input 4 are $\theta_{ON,4}$ = 0.22 rad and $\theta_{OFF,4}$ = 2.53 rad. The next cycle, Input 3 has the same turn on and turn off times that Input 4 had previously, and vice versa. The controller turns an input on at a specific instance each cycle; however, the controller alternates which input is switched on from one cycle to the next. Each input produces approximately the same voltage and current because they are exposed to the same level of solar irradiance. When these inputs are connected for different lengths of time, more current is drawn from one than the other, creating an imbalance. By switching between inputs, the controller is actively working to balance voltage inputs. While the design of the inverter topology prevents capacitor imbalance issues, the control strategy responds

to the dynamic operation of the inputs making the inverter more robust under balanced and imbalanced conditions.

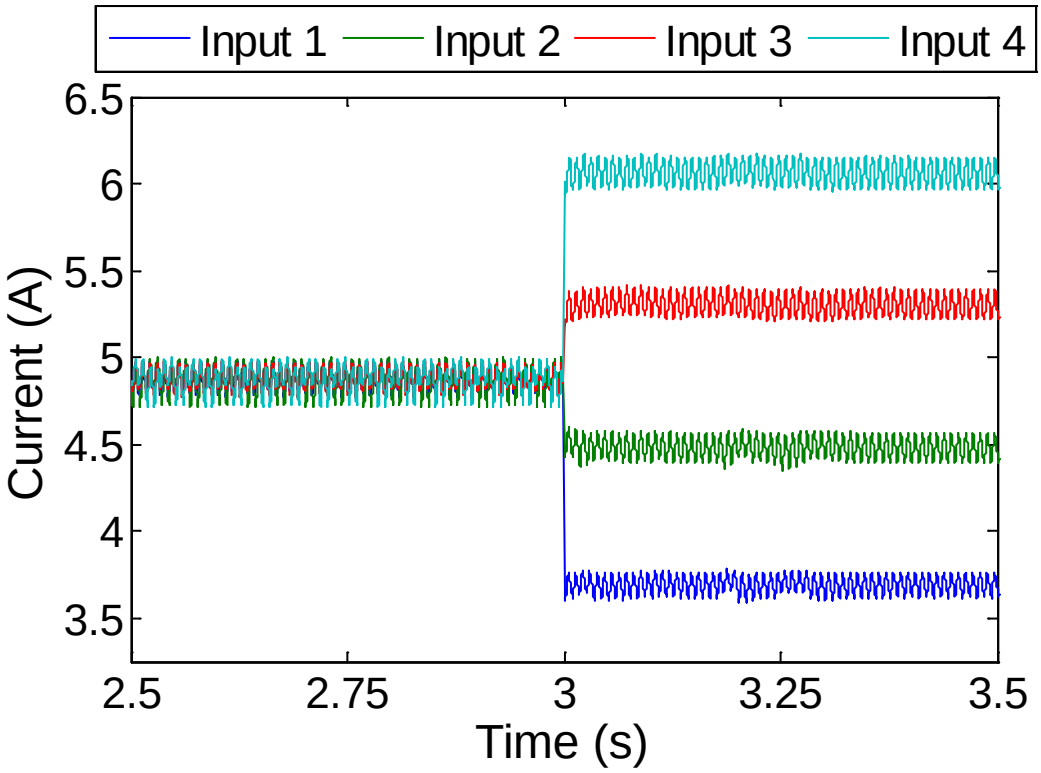

Figure 4.7: Inverter's response to different input conditions as shown through current drawn from PV inputs

Additionally, the inverter reacts quickly to changing conditions. In several simulations, the levels of solar irradiation were changed rapidly – in less than one cycle. The inverter responded almost immediately in every case, changing its output parameters in attempt to push the PV modules to operate near their MPP's. In all but the extreme cases, the controller was able to stabilize the operation of the inverter quickly. Figure 4.7 shows the output current of each PV module. At t = 3 s, the input conditions change from those in Scenario 3 (all 625 W/m^2) to those in Scenario 4 (evenly distributed between 475 W/m^2 and 775 W/m^2). The change elicits an

immediate drop in the output current of each PV module, but the controller quickly determines the optimal operating conditions and adjusts its output to push the PV modules towards their MPP. The PV modules are stable and operating near their expected MPP within 20 cycles, or roughly 0.33 s, of the inputs being changed.

5 Conclusion

Several strategies used to convert DC to AC are discussed. An emerging and promising topology is reviewed, and a novel control strategy is introduced to produce a sinusoidal output. The proposed strategy aims to maximize the amount of power drawn from each PV input and minimize the harmonic distortion and reactive power injected into the grid. A computer module of the single-phase inverter is developed to test the performance of the controller. The model uses four independently operating PV modules as separate input voltage sources, and the performance of the proposed inverter is compared to that of a comparable VSI inverter. While both inverters produce similar levels of power under balanced conditions, the proposed inverter produces more power under unbalanced conditions. The simulation results indicate that the proposed inverter is more effective in minimizing the harmonic content in the output waveform and reducing the reactive power injected into the grid.

Additional control strategies and minor adjustments to the topology could be made that would likely improve the performance of the inverter. The controller could use pulse-width modulation in lieu of the low-frequency technique presented in this paper. The former is a common control strategy used in many PV applications that would likely improve the performance of the controller at the expense of increasing its complexity. The use of PWM would eliminate the low-frequency harmonics in the output, and a LCL filter could be used instead of a single inductor to reduce the size of inductors required while satisfactorily removing the harmonic distortion.

The control strategy associated with the unique topology proposed has been successfully proven with a relatively small number of independent PV modules. These independent modules are approximately the same size as commercially available PV panels. Further research is needed to test the capabilities of the inverter with significantly more independent PV modules operating at lower voltages. Processing power, physical size and time constraints are all factors that need

to be accounted for when evaluating the performance of the inverter with a larger number of input PV systems.

The MPPT technique used in these simulations proved to be a weak point in the system. A dynamic MPPT technique is suggested for future research. A dynamic technique would be more accurate and responsive. It would improve the quality of the data delivered to the controller, which would likely improve the performance of the inverter.

APPENDIX A

MODEL: GS-P-280-Fab1

Grape Solar™
Clean Power. Today.

High Efficiency Poly-crystalline
Photovoltaic Module

Intertek

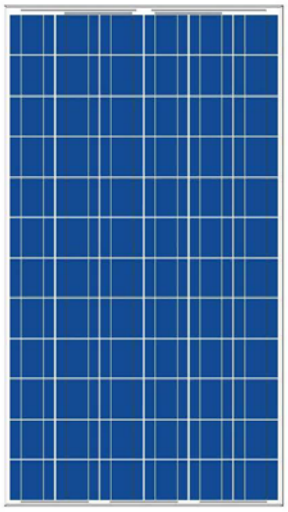

Overview

- High efficiency solar cells (approx. 18%) with quality silicon material for high module conversion efficiency and long term output stability and reliability.
- Positive power output tolerance from 0% to +3%.
- Rigorous quality control to meet the highest international standards.
- High transmittance, low iron tempered glass with enhanced stiffness and impact resistance.
- Unique frame design with strong mechanical strength for greater than 50 lbs/ft^2 wind load and snow load withstanding and easy installation.
- Advanced encapsulation material with multilayer sheet lamination to provide long-life and enhanced cell performance.
- Outstanding electrical performance under high temperature and weak light environments.

Applications

- Any large or small on-grid /off-grid solar power stations.
- Commercial/industrial building roof-top and ground systems.
- Residential roof-top and ground systems.

Warranty

- 10 year limited product warranty on materials and workmanship.
- 25 year warranty on >80% power output and 10 year warranty on >90% power output.
- Refer to warranty document for detailed warranty information.

Certifications

- ETL UL-1703 ISO 9000:2000
- CE TUV IEC61215 IEC61730

TÜV IEC ISO CE

Mechanical Specifications

Characteristic	Details
Cell Size	156mm x 156mm (6.14" x 6.14")
Module Dimension (L x W x T)	1956mm x 992mm x 50mm (77.0" x 39.1" x 2.0")
No. of Cells	6 x 12 = 72
Weight	23.2 kg (51.0 lbs)
Cable Length	950mm (37.4") ~ 1100mm (43.3")
Type of Connector	MC-IV
Junction Box	IP65 Rated
No. of Holes in Frame	4 draining holes, 8 installation holes, 2 grounding holes, 16 air outlet holes.

Rev.02• 0811

MODEL: GS-P-280-Fab1

Electrical Specifications
(STC* = 25 ºC, 1000W/m^2 Irradiance, and AM=1.5)

Model	GS-P-280-Fab1
Max System Voltage (IEC/UL)	1000V / 600V
Maximum Power P_{max}	280 W (0%, +3%)
CEC PTC Rating	251.0 W
Voltage at Maximum Power Point V_{mpp}	35.8 V
Current at Maximum Power Point I_{mpp}	7.82 A
Open Circuit Voltage V_{oc}	44.6 V
Short Circuit Current I_{sc}	8.43 A
Module Efficiency (%)	14.5%
Temperature Coefficient of V_{oc}	-0.156 V/ºC (-0.35% /ºC)
Temperature Coefficient of I_{sc}	5.06x10^{-3} A/ºC (0.06% /ºC)
Temperature Coefficient of P_{max}	-1.26 W/ºC (-0.45% /ºC)

*Standard Test Conditions

Physical Specifications mm (inch)

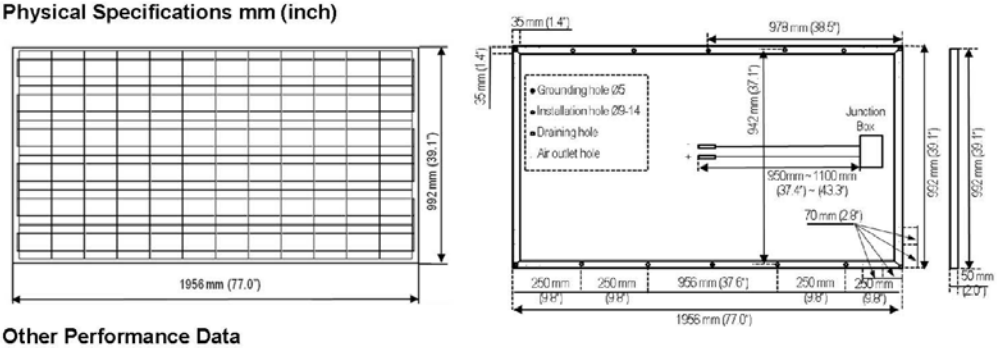

Other Performance Data

Power Tolerance	Operating Temperature	Max Series Fuse Rating	NOCT*
0%, +3%	-40 ºC to +85 ºC	15 A	45 ºC ± 2 ºC

*Normal Operating Cell Temperature

www.GrapeSolar.com

For service or support call

1-541-349-9000

Grape Solar™
Clean Power. Today.

1305 South Bertelsen Road
Eugene, Oregon 97402, USA
Tel: 541.349.9000 Fax: 541.343.9000

Rev.02• 0811

REFERENCES

1. Pazheri, F.R.; Al-Arainy, A.A.; Otham, M.F.; Malik, N.H.. “Global renewable electricity potential.” GCC Conference and Exhibition, 2013 7th IEEE, pp. 59-63. 17-20 November 2013.
2. The Shift Project. “World Electricity Production from All Energy Sources in 2011 (TWh)” http://www.tsp-data-portal.org/Breakdown-of-Electricity-Generation-by-Energy-Source?select=ELPRODP_Unit%2C%22%22TWh%22%22&select=ELPRODP_Year%2C%22%222011%22%22#tspQvChart
3. International Energy Agency. Monthly Electricity Statistics. May 2014. http://www.iea.org/media/statistics/surveys/electricity/mes.pdf
4. Williams, Richard. “Becquerel Photovoltaic Effect in Binary Compounds.” The Journal of Chemical Physics, Vol. 32, No. 5. May 1960.
5. Perlin, John. “The Silicon Solar Cell Turns 50.” NREL Report No. BR-520-33947. August 2004.
6. Chaniago, Krismadinata; Rahim, Nasrudin Abd.; Ping, Hew Wooi; Selvaraj, Jeyraj. “Photovoltaic module modeling using Simulink/Matlab.” Procedia Environmental Sciences Volume 17 (2013) 537 - 546.
7. Nedumgatt, Jacob James; Jayakrishnan, K. B.; Umashankar S.; Vijayakumar D.; Kothari, D.P.. “Perturb and Observe MPPT Algorithm for Solar PV Systems – Modeling and Simulation.” 2011 Annual IEEE India Conference (INDICON). 16-18 Dec. 2011.
8. Boonmee, C. and Kumsuwan, Y.. "Modified Maximum Power Point Tracking Based on Ripple Correlation Control Application for Single-Phase VSI Grid-Connected PV Systems." 10th International Conference on Electrical Engineering/Electronics, Computer, Telecommunications and Information Technology (ECTI-CON). May 2013.
9. Li, Jiyong and Wang, Honghua. “Maximum Power Point Tracking of Photovoltaic Generation Based on the Fuzzy Control Method.” International Conference on Sustainable Power Generation and Supply (SUPERGEN). 6-7 April 2009.
10. Lin, Whei-Min; Hong, Chih-Ming; Chen, Chiung-Hsing. “Neural-Network-Based MPPT Control of a Stand-Alone Hybrid Power Generation System.” IEEE Transactions on Power Electronics, Vol. 26, Issue 12, pp. 3571-3581. December 2011.
11. VanderMeulen, Aaron and Maurin, John. “Current source inverter vs. Voltage source inverter topology.” Eaton Technical Data TD02004004E. August 2010.
12. Krein, Philip T.. “Elements of Power Electronics.” Oxford University Press, Inc., New York. 1998.
13. Nabae, Akira; Takahashi, Isao; Akagi, Hirofumi. “A New Neutral-Point-Clamped PWM Inverter.” IEEE Transactions on Industry Applications, Vol. 1A-17, No. 5, pp. 518-523. September/October 1981.
14. Sivasankari, S. and Balarmurugan, C. R.. “Fifteen Level Cascaded Multilevel Inverter Using Embedded Controller.” International Journal of Information Science and Intelligent System, Vol. 3, No. 1. 2014.
15. Villanueva, Elena; Correa, Pablo; Rodríguez, José; Pacas Mario. “Control of a Single-Phase Cascaded H-Bridge Multilevel Inverter for Grid-Connected Photovoltaic Systems.” IEEE Transactions on Industrial Electronics, Vol. 56, No. 11. November 2009.

16. Daher, Ségio; Schmid, Jürgen; Antunes, Fernando L. M.. “Multilevel Inverter Topologies for Stand-Alone PV Systems.” IEEE Transactions on Industrial Electronics, Vol. 55, No. 7. July 2008.
17. Cavalcanti, Marcelo C.; Farias, Alexandre M.; Oliveira, Kleber C.; Neves, Francisco A. S.. “Eliminating Leakage Currents in Neutral Point Clamped Inverters for Photovoltaic Systems.” IEEE Transactions on Industrial Electronics, Vol. 59, No. 1. January 2012.
18. Rosas-Caro, Julio C.; Ramirez, Juan M.; Valderrabano, Antonio. “Voltage Balancing in DC/DC Multilevel Boost Converters.” 40th North American Power Symposium. Sept. 2008.
19. Huang, Jing and Corzine, Keith A.. “Extended operation of flying capacitor multilevel inverters,” IEEE Trans. Power Electron., vol. 21, no. 1, pp. 140–147. January 2006.
20. Trabelsi, M. and Ben-Breham, L.. "DEVELOPMENT OF A GRID CONNECTED PHOTOVOLTAIC POWER CONDITIONING SYSTEM BASED ON FLYING CAPACITORS INVERTER." 8th International Multi-Conference on Systems, Signals & Devices. 2011.
21. Celanovic, Nikola. “Space vector modulation and control of multilevel converters,” Ph.D. dissertation. Virginia Polytechnic Inst. State Univ., Blacksburg, VA. 2000.
22. Lai, Jih-Sheng and Peng, Fang Zheng. “Multilevel Converters – A New Breed of Power Converters.” IEEE Transactions on Industry Applications, Vol. 32, No. 3. May/June 1996.
23. Najafi, E.; Yatim, A. H. M.; Samosir, A. S.. “ A New Topology – Reversing Voltage (RV) – for Multi Level Inverters.” 2nd IEEE International Conference on Power and Energy (PECon 2008), pp. 604-608. 1-3 December 2008.
24. Müller, J.. “Assessment and Optimisation of Step-Inverters for Photovoltaic Systems (Untersuchung und Optimierung von Stufeninvertern für Photovoltaik-Anlagen, in Germen).” Ph.D. Dissertation. Fernuniversität-Gesamthouchschule Hagen. 1994.
25. Nordvall, Andreas. “Multilevel Inverter Topology Survey.” Master of Science Thesis in Electric Power Engineering. Chalmers University of Technology, Göteborg, Sweden. 2011.
26. Calais, Martina and Agelidis, Vassilios G.. “Multilevel Converters for Single-Phase Grid Connected Photovoltaic Systems – An Overview.” IEEE International Symposium on Industrial Electronics. pp. 224-229. 7-10 July 1998.
27. Joshi, Hemant; Tekwani, P. N.; Hunduja, Amar. “Implementation of a Five-Level Inverter Using Reversing Voltage Topology: A Competitive Solution for High-Power IM Drive Application.” Indian Institute of Technology, Roorkee. 2010.
28. Scholten, David M.; Ertugrul, N.; Soong, W. L.. “Micro-Inverters in Small Scale PV Systems: A Review and Future Directions.” Australian Universities Power and Engineering Conference, AUPEC 2013. Hobart, TAS, Australia. 29 September – 3 October 2013.
29. Kramer, W.; Chakraborty, S.; Kroposki, B.; Thomas, H.. “Advanced Power Electronic Interfaces for Distributed Energy Systems Part 1: Systems and Topologies.” Technical Report, National Renewable Energy Laboratory. March 2008.
30. Sera, Dezso and Baghzouz, Yahia. “On the Impact of Partial Shading on PV Output Power.” 2nd WSEAS/IASME International Conference on Renewable Energy Sources (RES ’08). Corfu, Greece. 26-28 October 2008.
31. Barreiro, Carlos; Jansonn, Peter M.; Thompson Andrew; Schmalzel, John L.. “PV By-Pass Diode Performance in Landscape and Portrait Modalities.” 37th IEEE Photovoltaic Specialists Conference (PVSC), pp. 3097-3102. 19-24 June 2011.

32. Yongli, Zhu; JianGuo, Yao; Di, Wu. “Comparative study of two stages and single stage topologies for grid-tie photovoltaic generation by PSCAD/EMTDC.” International Conference on Advanced Power System Automation and Protection (APAP), Vol. 2, pp. 97-100. 16-20 October 2011.
33. Tomova, Angelina. “Grid Connected PV Inverter Topologies An Overview.” DERlab Young researchers and PhD seminar – Distributed generation and renewable energy sources. Glasgow, UK. 07 April 2011.
34. Blaabjerg, F.; Chen, Z.; Kjaer, S.. “Power Electronics as Efficient Interface in Dispersed Power Generation Systems.” IEEE Transactions on Power Electronics, Vol. 19, No. 5, pp. 1184-1194. September 2004.
35. Shmilovitz, Doron and Levron, Yoash. "Distributed Maximum Power Point Tracking in Photovoltaic Systems - Emerging Architectures and Control Methods." Automatika – Journal for Control, Measurement, Electronics, Computing and Communication, Vol. 53, No. 2. 2012.
36. IEEE Standard 519- 1992. “IEEE Recommended Practices and Requirements for Harmonic Control in Electrical Power Systems.” The Institute of Electrical and Electronics Engineers, Inc., New York. 1993. pp. 73.
37. Denherder, Tyson. “Design and Simulation of Photovoltaic Super System Using Simulink.” Senior Project, California Polytechnic State University. 2006
38. Nikhil, P. G. and Subhakar, D.. "An Improved Simulation Model for Photovoltaic Cell." International Conference on Electrical and Control Engineering (ICECE), pp. 1978-1982. 16-18 September 2011.
39. Xiao, Weidong; Dunford, William G.; Capel, Antoine. “A Novel Modeling Method for Photovoltaic Cells.” IEEE 35th Annual Power Electronics Specialists Conference (PESC 04), Vol. 3, pp. 1950-1956. 20-25 June 2004.
40. Townsend, T.U.. “Simplified Performance Modeling of a Direct-Coupled Photovoltaic System.” Master's Thesis, University of Wisconsin-Madison. 1989.
41. Dimitrijev, Sima. “Principles of Semiconductor Devices.” Oxford University Press, Inc., New York. 2006.

VITA

Martin Prichard was born in Lexington, Kentucky. He obtained his Bachelor of Science degree in Physics-Engineering from Washington and Lee University in 2011. He earned a graduate certificate from the Power and Energy Institute of Kentucky in 2013 while enrolled at the University of Kentucky. Martin worked as a Research Engineer at Innovative Energy Solution prior to assuming his current engineering role with LG&E and KU.